CHAPTER 4

THE CHEMICAL SENSOR ARRAY

4. THE CHEMICAL SENSOR ARRAY

4.1 INTRODUCTION

This chapter is focused on the electronic properties of PPy thin films and on the development of a chemical sensor array based on this material. After achieving the PPy thin film synthesis and the iodine doping, it is necessary to study its electrical behaviour. Generally, the four-point probe method is considered to be the most accurate technique to determine the electrical characterization of polymers.[1-4] In the first part, in order to be able to measure the conductivity, a new kind of four-point probe configuration has been designed. Then, resistivity measurements on plasma polymerized PPy thin films iodine doped have been performed. Additionally, the design of a gas chamber for studying the polymer-vapour interactions has been described. At last, the analysis of a vapour based on the system developed has been carried out.

Probably, one of the most difficult tasks which were necessary to deal with was how to measure the electrical conductivity in our samples. A brief introduction about conductivity measurements is given next to understand the choice of the four point probe method as the technique employed to study conductivity on PPy thin films.

Conductivity is defined as the ability of a substance to conduct electrical current. It is commonly represented by σ and has the SI units of Siemens per metre ($S \cdot m^{-1}$). In addition, conductivity is the reciprocal of electrical resistivity (ρ, the SI unit is the ohm metre $\Omega \cdot m$).

Electrical resistivity or volume resistivity is a measure of the leakage current directly through a material. When measuring the volume resistivity, the test sample is placed between the two electrodes and a potential difference is applied between them. The resulting current is distributed through the volume of the test sample and it is measured. The resistivity is calculated from the geometry of the electrodes and the thickness of the sample:

$$\rho = \frac{K_v}{t} \times \frac{V}{I} \tag{1}$$

where: K_v= test cell constant for volume resistivity based on cell geometry (cm^2)
V = applied voltage (V)
I = measured current (A)
t = sample thickness (cm)

Figure 1 shows a system for testing the resistivity of a bulk material such as a metal bar or rod. The current source is connected to both ends of the sample. The voltmeter leads are placed a known distance apart. The resistivity is calculated from the cross-sectional area of the sample and the distance between the voltmeter leads:

$$\rho = \left(\frac{V}{I}\right) \times \left(\frac{A}{L}\right) \tag{2}$$

where: A = cross sectional area of sample (w x t) in cm^2
L = length of distance between voltmeter leads in cm

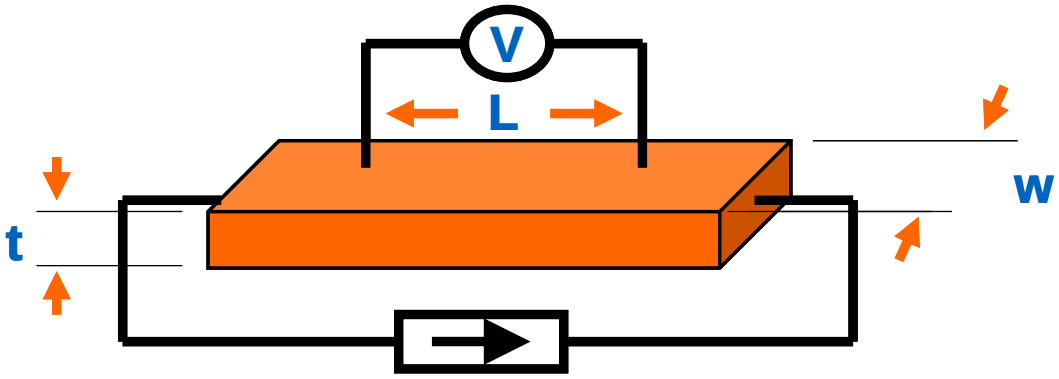

Figure 1. Resistivity measurement system of conductive materials.

Besides, with the emergence of micro/nanostructured materials, such as conducting polymers, and the continuing decrease of feature sizes of electronic circuitry, the conducting properties in such a minute scale has become an important issue. Sheet resistance is a measure of resistance of thin films that have a uniform thickness instead of using volume resistivity.

According to equation 2 and if *W* is the width of the sample and *t* its thickness, then the resistance can be written:

$$R = \frac{V}{I} = \left(\frac{\rho}{t}\right) \times \left(\frac{L}{W}\right) \tag{3}$$

where $\rho_s = \left(\frac{\rho}{t}\right)$ is the sheet resistance of a layer of the material.

The unit for sheet resistance should be the ohm, since L/W is unitless. However, to distinguish this number from the measured resistance $\left(V/I\right)$, it is customary to refer to it as “ohms per square”.

As commented before, the most common technique used to measure resistivity in semiconductors or thin films is the four-point probe method. The set-up consists of four-point collinear probes, where a constant current is applied in the two outer probes and the voltage drop is measured in the inner probes. Then, the sheet resistivity is given by equation 4, where CF is the correction factor based on the ratio of the probe to wafer diameter and on the ratio of wafer thickness to probe separation.

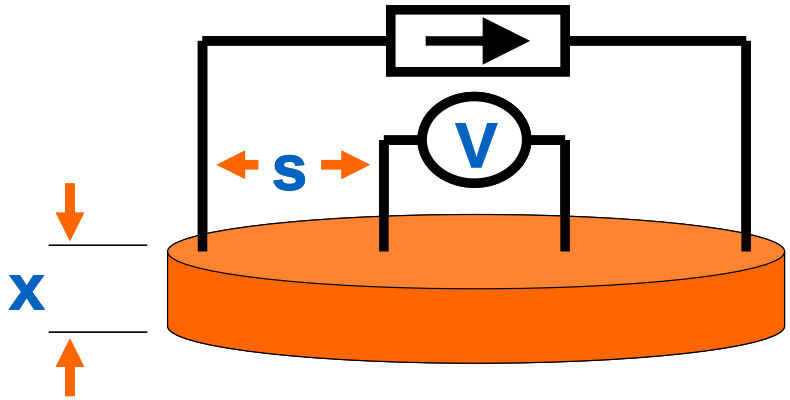

Figure 2. Schematic four-point probe configuration for measuring sheet resistivity.

$$\sigma = \left(\frac{V}{I}\right) * CF \tag{4}$$

If the sample is of semi-infinite volume and the interprobe spacing are s1 = s2 = s3 = s, then it can be shown that the resistivity of a semi-infinite volume is given by:

$$\rho = 2\pi \times s \times \left(\frac{V}{I}\right) \tag{5}$$

Because samples are finite size, Valdes[5] calculated the correction factor for six different boundary configurations. He concluded that if the distance from any probe to the nearest boundary is at least 5s, no correction factor is required. Therefore, for sample thickness equal or lower to 5s, the resistivity is calculated according equation 6.

$$\rho = a \times 2\pi \times s \times \left(\frac{V}{I}\right) \tag{6}$$

where a = thickness correction factor

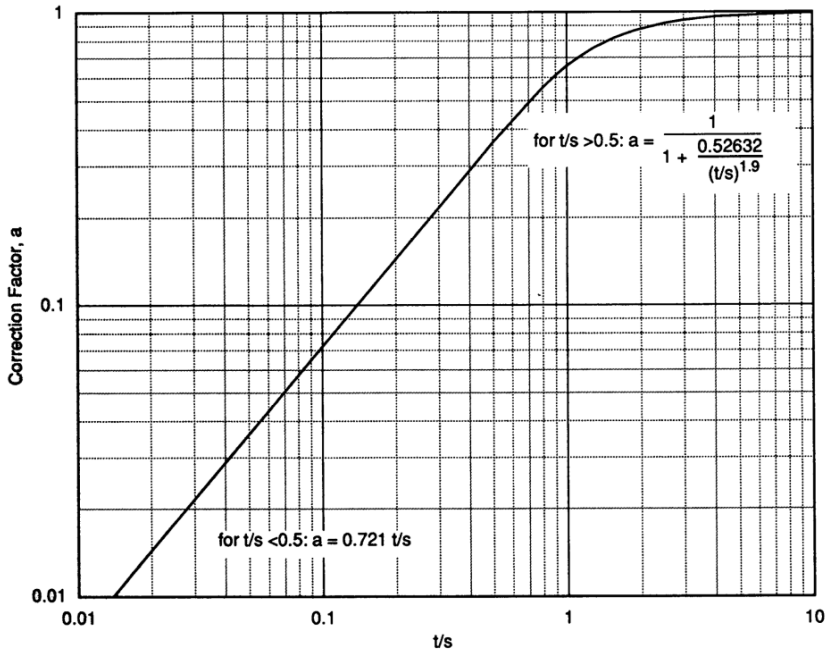

Figure 3. Thickness correction factor according to Valdes.[5]

Thickness correction factor is plotted in Figure 3. It can be observed that for $t/s \geq 5$, *a* = 1, and that for $t/s \leq 0.5$ the curve behaves as a straight line. Thus, *a* can be obtained by calculating the slope. Hence, for samples thickness equal to or less than one half the probe spacing, $a = \frac{1}{2Ln2} \times \frac{t}{s}$. When this value is introduced into equation 6, the following equation is obtained:

$$\rho = \frac{\pi}{Ln2} \times t \times \frac{V}{I}, \qquad t/s \leq 0.5 \tag{7}$$

Finally, dividing both sides by *t*:

$$\rho_s = \frac{\pi}{Ln2} \times \frac{V}{I}, \quad t/s \leq 0.5 \tag{8}$$

By using this equation the sheet resistivity (ohms per square) is obtained. Moreover, it should be note that ρ_s is independent of the sample geometry and that only depends on the studied material.

Therefore, because we are dealing with thin films, the four-point probe method seems to be an excellent system to study PPy conductivity.

4.2 EXPERIMENTAL PART

4.2.1 PLASMA POLYMERIZATION

The plasma reactor was evacuated to a base pressure of 0.04 mbar, then, pyrrole was introduced and the working pressure was set at 0.08 mbar. Polymerization time ranged from 1 to 30 min. The power during the polymerization was set at 20 W, with a 90% duty cycle. Finally, samples were left in an iodine chamber to carry out the doping process. The time of doping varied from 20 to 100 min.

4.2.2. METHODS AND EQUIPMENTS

The resistance measurements for the probe testing were performed using a SOLARTRON 1260 impedance analyzer which is controlled trough GPIB by a LabVIEW 5.1 program. The impedance of the electrodes was measured over a frequency range of 1 to 1000 Hz.

A Keithley 2611 System SouceMeter was used for four-point probe conductivity measurements, since it can be used as a constant current source and as a voltammeter at the same time.

AFM images were acquired with an XE-100 (PSIA Inc.) with lateral resolution of 0.15 nm and vertical of 0.05 nm, by non-contact mode. Images were analyzed by XEP and XEI software for data acquisition and image processing.

The water vapour was introduced into the gas chamber by using an evaporator (Bronkhorst CEM, Liqui-Flow). An initial flow of 0.5 g/h was established and then, the maximum flow allowed (2 g/h) was applied.

For CO_2 gas measurements, an Erlenmeyer containing dry ice was connected to the gas chamber through one of the gas inlets. CO_2 was introduced into the chamber by sublimation. It was left to saturate the compartment by displacing the air and for that purpose it was purged twice until reaching the saturation level.

For the adsorption-desorption cycles, the CO_2 was left to go inside the chamber for 10 min until reaching the saturation level. Then, the gas chamber was open to air for 20 min to let the molecules get desorbed until reaching a steady resistance value.

4.3 FOUR-POINT PROBE DESIGN

4.3.1 MOTIVATION

Because of the continuously reduction in size of electrical components, nanotechnology has to overcome the difficulties related to working at such small scale. Different attempts have been performed to measure conductivity in several types of materials. Conducting Atomic Force Microscopy (C-AFM) has been used in the study of ITO films[6] or in DNA conductivity.[7] Nevertheless, one of the problems associated to this kind of technique is the parasitic capacitance associated in these measurements. This unwanted effect can be avoided by using the four-point probe technique. Due to the fact that current between the inner probes is practically zero, the contact resistance can be neglected.

According to this, several research groups have chosen this method to work with and even they have designed their own four-point probe array. Keller *et al* have reported the fabrication of a microscopic four-point probe with a spacing of about 15 μm among the probes by a micromachining process.[8] Ju *et al* have managed to reduce the separation among electrodes to 1 μm by modifying an AFM probe using a focused ion beam system (FIB).[9] Similar electrode spacing can be constructed using microfabrication of these probes by photolithography.[10] However, for all these systems there are some drawbacks that need to be improved. One of the key factors in resistance measurements is the contact between sample and probe. For instance, achieving a proper ohmic contact in the junction is highly important for the development of diodes.[11] On the other hand, an excessive force in the contact pressure can lead to an irreversible damage in the probe or, even, in soft samples, especially polymers.

Because all this, it was decided to design a new four-point probe configuration. In most cases, the four-point probes are mounted on a like-clip system which approaches to the surface to determine the resistivity. As stated before, due to this movement, the polymeric surface or the probes can get damaged. Therefore, the proposal to solve this problem is to perform the polymer deposition directly on the probes. Instead of depositing the polymer on a surface and then measuring the electrical resistance, it would be more convenient to design a surface with the probes incorporated on it and then to deposit the polymer onto them.

One of the problems related to this system could be the probes maintenance. Using the same surface with the probes incorporated for different experiments entails the total thin film removal from the last experiment. Otherwise, there could be a contamination problem among samples. Moreover, probes could get damaged either by the deposition technique employed (etching in case of plasma) and by solvents employed cleaning the surface.

The solution proposed is also linked with the idea of a rapid, easy and cheap essay to measure conductivity on polymeric thin films: to use a circuit print board integrated with the four-point probe. It solves maintenance problems since it is possible to use one circuit print board per each sample. Mass fabrication of printed circuit boards is not so expensive and it can be compensated by the fact of using always a new system. Furthermore, measurements are easily performed as the leads in a printed circuit board can be connected to almost any voltmeter.

Thereby, the plan is to design a new four-point probe configuration incorporated into a printed circuit board to measure the conductivity on plasma polymerized PPy thin films.

4.3.2 PROBE CONFIGURATION TEST

In the attempt to find a suitable four-point probe configuration, several kinds of electrodes were tested. These electrodes correspond to typical configurations employed frequently in electronics. The probe geometry can be classified into four-point probe, two-point probe and interdigital probe. Additionally, there are different models concerning area and separation among probes (Figure 4). The purpose is to study the correlation between these parameters and the resistance to determine which the most critical factors are for designing the new array.

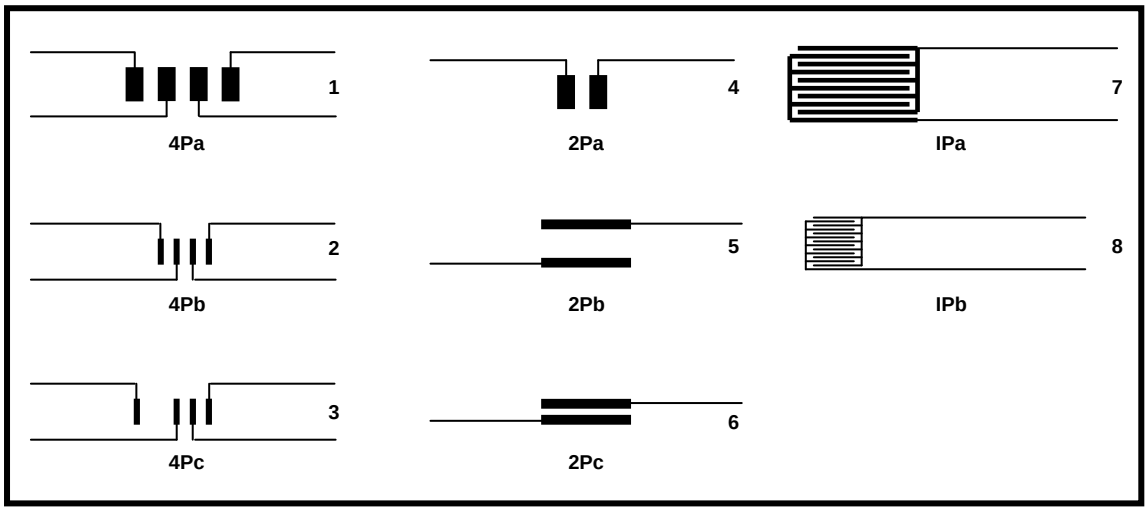

Figure 4. Schematic representation of the different probes used for the resistivity measurements. The four-point probes correspond to numbers 1, 2 and 3, and are named 4Pa, 4Pb and 4Pc respectively. The two-point probes correspond to numbers 4, 5 and 6, and are named 2Pa, 2Pb and 2Pc respectively. The interdigital probes correspond to number 7 and 8, and are named IPa and IPb respectively.

The three probes groups characteristics tested in the experiments are depicted as follows. There are three different kinds of four-point probe configurations, named 4Pa, 4Pb and 4Pc. The 4Pa electrodes have an active area of 2.00 x 1.00 mm and an electrode spacing of 0.90 mm. In 4Pb, the electrodes area measures 1.30 x 0.25 mm and the spacing 1.00 mm. The 4Pc has the same electrode area than 4Pb probe, but the spacing among probes is modified. The three closer electrodes are separated by 0.44 mm and the external one by 2.00 mm. Moreover, there are three different types of two-point probes: 2Pa, 2Pb and 2Pc. The 2Pa has an electrode geometry that measures 1.30 mm in length and 0.25 mm in width, and the distance between probes is 0.90 mm. The 2Pb consists of two 5.00 x 0.125 mm electrodes separated by 1.40 mm. In the 2Pc, the electrode area is the same as that of 2Pb and separation between probes is reduced to 0.20 mm. At last, two different interdigital probes are tested: IPa and IPb. IPa is composed by 10 electrodes, each of them with an area of 10.00 x 0.23 mm and separated by 0.31 mm, while IPb has 14 electrodes with an area of 5.00 x 0.135 mm and separated by 0.19 mm.

4.3.3 RESISTANCE MEASUREMENTS AND FINAL DESIGN

First of all, the resistance analysis for the uncoated electrodes was carried out with the purpose of acquiring a reference value to compare with further experiments. The resistance obtained was practically the same for the eight electrodes, and it was of $\sim 10^8\ \Omega$. It corresponds to the probe resistance in contact with air. Considering the high

electrical constant for air at atmospheric pressure (1.00059), any value close to 10^8 Ω can be classified as an insulator. Then, the results obtained for the electrodes are summarized in Table 1.

Table 1. Resistance measurements of the different probes.

	4Pa	4Pb	4Pc	2Pa	2Pb	2Pc	IPa	IPb
R [Ω]	10^8	10^8	10^8	10^8	10^8	10^7	$9{\cdot}10^5$	10^5

A 190 nm thick PPy film was deposited on every electrode and samples were placed in the iodine chamber for 40 min to carry out the doping process. The resistance for 4Pa, 4Pb, 4Pc, 2Pa and 2Pb is 10^8 Ω, which coincides with the base value obtained previously. Despite achieving the PPy deposition and the iodine doping, no electrical signal flows among probes. In contrast, the 2Pc resistance has decreased one decade. Additionally, interdigital probes have shown the lowest resistance: $9{\cdot}10^5$ and 10^5 Ω for IPa and IPb respectively.

The different values obtained are due to the probe configuration since the experimental conditions have been the same for all the samples. Thus, the electrode area, the probe spacing and the design should be analyzed to conclude which factors related to conductivity measurement are important. This way, it will be possible to design the new electrode configuration.

According to the results found, it seems that the most important factor to get a low resistivity depends on probe spacing. Electrodes with a resistance of 10^8 Ω have a probe spacing which ranges from 0.90 to 2.00 mm. On the other hand, the rest of electrodes, which show a lower resistance, have a probe spacing which ranges from 0.19 to 0.31 mm. Charge transport in conducting polymer is ruled by the probability of hopping transport, which is the phenomenon of charge carriers passing from one molecule to another.[12-15] This charge transport is associated to electron jumping in crystalline ordered regions of the polymer. It is in these ordered regions where the conduction electrons are three-dimensionally delocalizated and can diffuse through chains.

Related to conductivity in the studied electrodes, it seems that more separated probes make the charge carrier transport more difficult. Different electronic pathways for electron hopping should be available to get an electron flow among probes. Thus, when there is an excessive separation among them, there is no current flowing through

the electrodes probably due to chain defects and amorphous structure associated to plasma polymerization. Summing to this effect a low polymer thickness, large separation distances among probes still makes the charge transport more difficult.

As a consequence, IPb, the electrode with the shortest probe spacing (0.19 mm), has the lowest resistivity (10^5 Ω). However, the second lowest resistivity corresponds to the IPa electrode, which has a larger probe spacing (0.31 mm) in comparison with 2Pc, whose probe spacing measures 0.20 mm. Related to this, it should be considered another factor apart from probe spacing to explain the change in resistivity. In this sense, it may be that probe geometry plays an important role also. In concrete, as it can be observed in Figure 4, IPa presents a higher surface area electrode compared with 2Pc. 2Pc consists of a typical two electrodes configuration, while the IPa has an interdigital configuration. An interdigital electrode consists of a pair band of array electrodes that mesh with each other. The resistivity difference can be explained in part by the interconnection of electrodes. The length of interdigital electrodes is much longer in comparison with the two point probe. Therefore, it can be assumed that because interdigital electrodes have a higher surface area electrode, there are more chances for electron transference.

Compiling resistivity measurements, two factors have been found to be critical in the electrode design. The first one is achieving the minimal probe spacing and the second one to work with high surface area probes. These two factors should be combined for the design of an optimal four-point probe configuration. Although the interdigital configuration has shown the best results, it can not offer the advantages of four-point probe measurements. Regarding the reasons explained in the introduction, this configuration allows working with samples independently of their geometry and thickness and the insensitivity to contact resistances is preserved.

According to the optimal features discussed above, a new four point probe configuration on a printed circuit board has been designed. The scheme of the new optimized electrode can be seen in Figure 5. Probes are conducting layers made of copper foil and measure 15 mm in length and 0.25 in width. The spacing probe has been fixed at 0.285 mm, the minimal distance that could be achieved in the circuit print board design for this configuration.

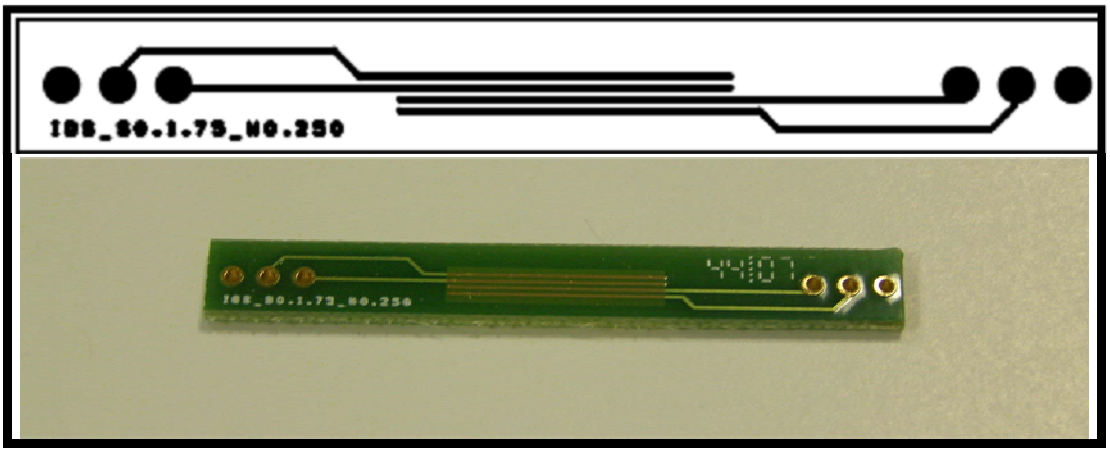

Figure 5. Scheme and picture of the four point probe design.

As it can be observed, the plasma polymerized PPy can be deposited directly on the probes. To perform electrical measurements, electrical contacts are soldered on the corresponding holes, which are connected to the intensity source and to the voltmeter. The current is applied to the outer probes and the voltage drop is measured in the inner probes.

4.3.4 POLYPYRROLE DEPOSITION

Once the probe parameters have been fixed and the new four point probe designed, PPy deposition on the probe surface has been investigated. Figure 6 shows the three stages in which the probe is involved for conductivity measurements. In the photo, the naked four point probe is labelled with number 1. Number 2 corresponds to a PPy plasma polymerized film deposited on the four point probe. Although it could be not well appreciated in the photo, the surface is shinier in comparison with the non-polymerized surface as a result of the PPy deposition. Nevertheless, the most important change can be appreciated in the four point probe labelled with number 3, which corresponds to a plasma polymerized film and iodine doped for 60 minutes. The polymer has turned into a darker colour due to the doping process. It is well-known that conducting polymers change their colour when they switch from their reduced state to the oxidized. For instance, PPy presents a transparent yellow colour in the reduced state, which fits with the colour observed in Figure 6 for the plasma polymerized sample. Furthermore, PPy after oxidation displays a black colour which fits again with the sample plasma polymerized and iodine doped. A change in the electronic state of

the polymer is associated with the colour change and it is a proof of having achieved the doping process.

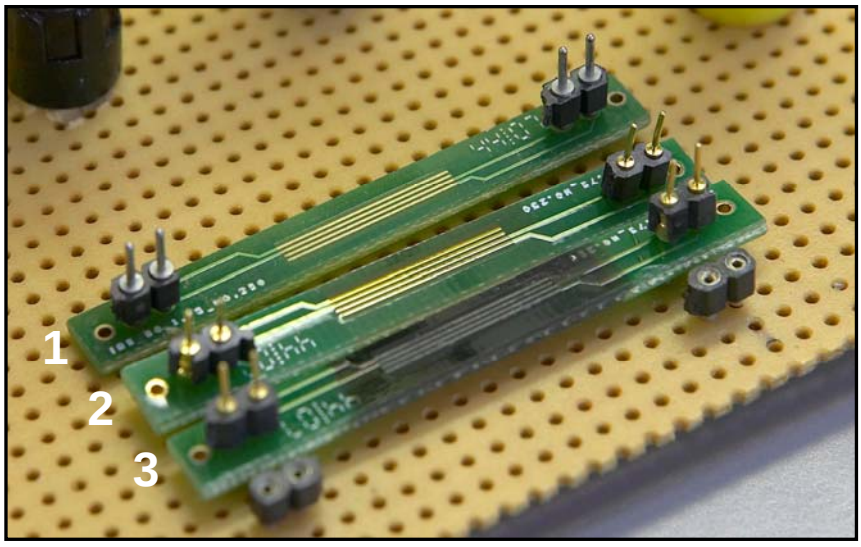

Figure 6. Picture of the four-point probe (1), four-point probe PPy plasma polymerized (2) and four-point probe PPy plasma polymerized and iodine doped (3).

Since probes were made of copper, the same polishing process than in Chapter 3 was carried out in order to work under the same experimental conditions than on plasma polymerization. Figure 7 displays an AFM image of one probe after polishing. The measured roughness is 12 nm which coincides with the obtained for copper surfaces in Chapter 3.

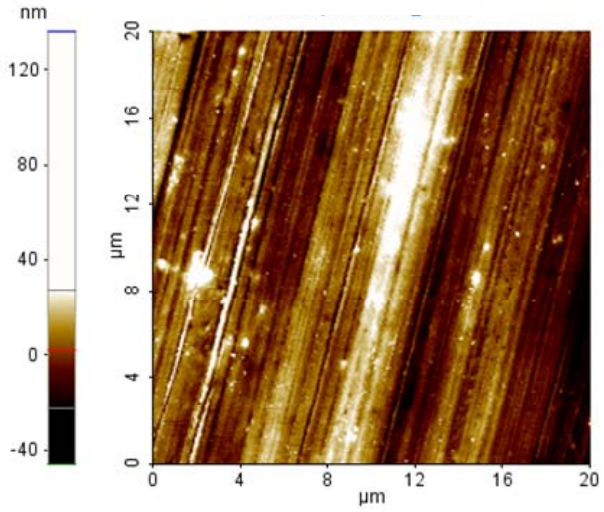

Figure 7. AFM image of the four point probe surface after polishing.

Afterwards, Figure 8 shows the probe surface after plasma polymerization. A PPy thin film was deposited on it. Moreover, the surface topography looks alike the PPy

deposition in Chapter 3. The same typical mountain features are observed, which means that the deposition process has not been affected by the surface. As a consequence, results from Chapter 3 can be extrapolated for the four point probe's material as well.

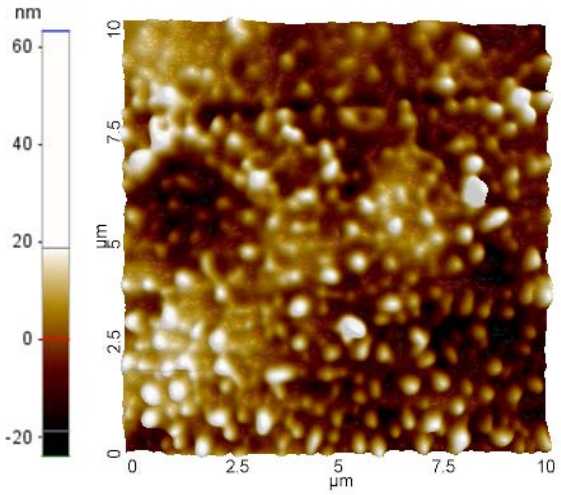

Figure 8. AFM image of a four-point probe in which a PPy plasma polymerized thin film has been deposited.

4.4 CONDUCTIVITY MEASUREMENTS

The conductivity measurements have been performed using the new four point probe configuration. Different experimental conditions have been tried in order to optimize the analysis measurements.

4.4.1 CURRENT SOURCE

The first experiment performed has been focused on looking for the adequate constant current source. Since organic thin films are being used, some problems associated with polymer stability can happen. Therefore, several currents have been applied to elucidate the optimal conditions.

Figure 9 provides sheet resistivity obtained from different current values. The current ranges from 1 µA to 10 mA. The more similar values can be found between 5 µA and 5 mA which seem to report the real resistivity value. At 1 µA, the resistivity is lower than the expected result. Nevertheless, current at the nanoampere range can be a little bit tricky, because at these levels, noise can be a problem. Moreover, internal impedances of the Keithley SourceMeter or circuit can be critical to ensure an accurate measurement. Therefore, current at such low levels should be better avoided. Additionally, the resistivity at 10 mA presents the lowest sheet resistivity value. Working with high currents can cause an overheating in polymeric thin films. In spite of the fact that conducting polymers are known as synthetic metals, they do not present a high thermal conductivity associated with metal properties. Thereby, depending on their internal resistance they can suffer from overheating. Moreover, this overheating can result in the polymer decomposition. Because of that, the resistivity measurement at 10 mA may be affected by overheating showing a lower value.

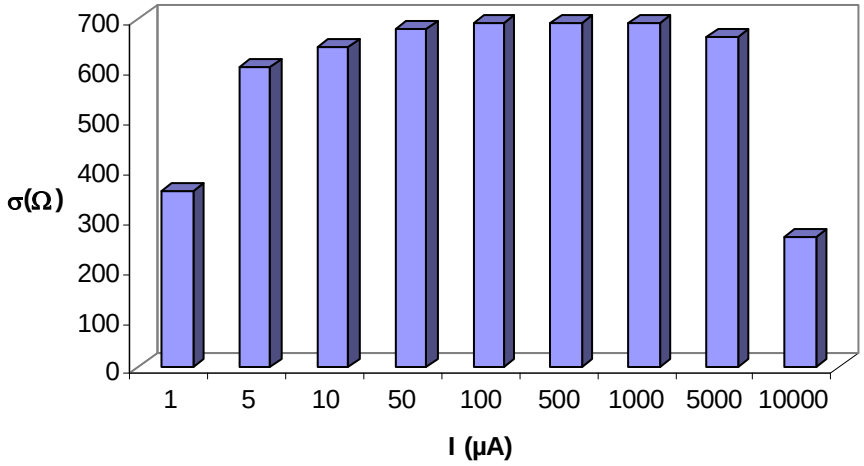

Figure 9. Sheet resistivity response under different current values.

The measured sheet resistivity on the plasma polymerized film is about 690 Ω per square and the optimal current range is placed between 5 μA and 5 mA because it is over this range that the Ohm's law is obeyed. This law postulates that the resistance is independent no matter the current that is being applied (Equation 9). Thus, the results which show a similar resistivity are thought to be the ones which accomplish this law.

$$I = \frac{V}{R} \tag{9}$$

Nonetheless, an observation at larger times scale was performed to continue investigating the current range.

4.4.2 RESISTIVITY Vs TIME

A further experiment was carried out in the sample used in the last section. Resistivity Vs time is measured to investigate the current range and studying the polymer stability.

Table 2. Sheet resistivity at different currents as a function of time.

days / I (μA)	Sheet Resistivity (Ω)					
	1	14	16	20	23	28
1	354	453	499	612	5711	6708
5	603	621	639	866	6119	6799
10	644	703	689	943	6209	6799
50	680	734	712	961	6028	6617
100	689	739	712	965	5892	7478
500	689	761	716	974	3218	4170
1000	689	761	716	974	1949	3037

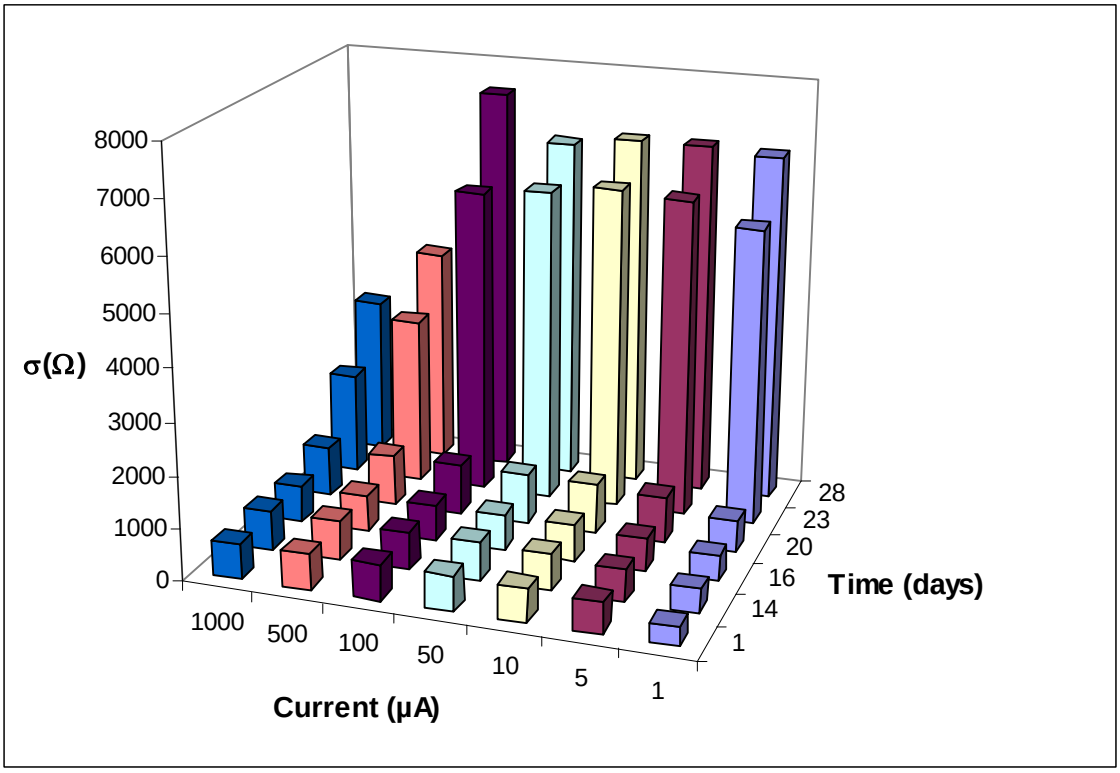

Figure 10. Representation of sheet resistivity at different currents as a function of time.

Figure 10 shows the resistivity evolution over time. It can be appreciated that after 23 days there is a sudden resistivity increase. During the first 20 days, there are few variations of resistivity. Thereby, it can be assumed a steady state for approximately 20 days, which is even longer than stability results found in other investigations.[16] From the 23th day, there is an important increase in resistivity of almost one decade. The observed increase could be attributed to polymer degradation. An oxidation process can affect to the PPy backbone and it could cause a loss on its electrical properties. Nevertheless, despite having increased the sheet resistivity after 4 weeks, the values obtained can be considered correct enough for electronic applications. For instance, Cruz *et al*[17] synthesized PPy plasma polymerized iodine doped films with a thickness between 4.9 and 19.8 μm and a conductivity between 10^{-9} and 10^{-3} S/cm. Films obtained in this work present conductivity values between 4 and 40 S/cm.

Furthermore, having a look to the currents some remarks should be done about the current range. Until the twentieth day, resistivity measurements from 10 μA to 1 mA show very similar values according to the aforestated results. However, from the twenty-third to the twenty-eighth day, currents which have similar values of resistivity ranges from 1 to 100 μA, probably due to the overheating and the degradation exposed

above. Because all that, it seems that the constant current to apply in future experiments should be fixed between 10 and 100 µA, since this range has provided values which accomplish Ohm's law for all the experimental conditions tested.

4.4.3 INFLUENCE OF DOPING TIME AND SELF-ASSEMBLY ON CONDUCTIVITY

To optimize the doping process, monitoring of polymeric films conductivity exposure to iodine vapor was performed. Samples were introduced into the iodine chamber as usual and every 20 minutes the probe was removed to measure the conductivity. Furthermore, one probe was modified by assembling of a Py12SeH SAM to compare the effect of the monolayer on conductivity. The results are presented in Figure 11.

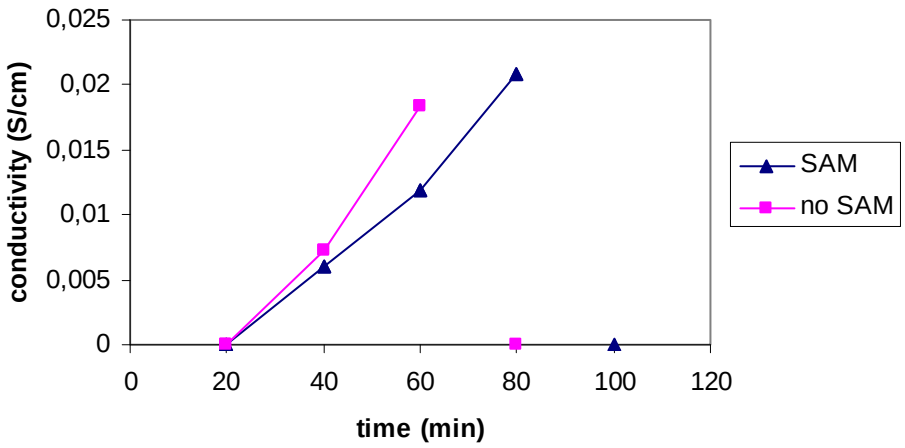

Figure 11. Conductivity evolution in function of exposure time to iodine of a 475 nm thick PPy plasma polymerized film Py12SeH SAM-modified four-point probe and a non-modified.

According to the above graph and other experiments carried out during the investigation, it was observed that, at least, the assembly of the monolayer has no a detrimental effect on conductivity. As the graph shows, there are no significant differences between SAM-modified and non-modified four-point probe. At 40 minutes of doping, conductivity for SAM-modified and non-modified samples are $6.0 \cdot 10^{-3}$ and $7.1 \cdot 10^{-3}$ S/cm, and at 60 minutes $1.1 \cdot 10^{-2}$ and $1.8 \cdot 10^{-2}$ S/cm. Numerous studies have attempted to explain the conduction mechanism through monolayers.[18-22] Mainly, the electron transference process has been divided into two possibilities: tunnelling and hopping. Although, according to the same studies the most likely option for alkanethiol monolayers is tunnelling. As a matter of fact, it is assumed that the Fermi levels of the electrodes, which are intimately related to conductivity properties, lie between the

HOMO (highest occupied molecular orbital) and LUMO (lowest unoccupied molecular orbital) gap. Although that, others conduction mechanisms can not be excluded. Furthermore, because PPy is deposited onto the SAM and electrode surface and the conductivity mechanism in polymers is ruled by hopping transport, it can be hypothesized that this transport has an important role in the electron transference process also. As a consequence, this finding suggests that SAM-modified electrodes can be used for electrical measurements without causing an important loss of conductivity.

On the other hand, there are strange variations on conductivity from minute 60. For instance, at 80 minutes of iodine exposure, the SAM-modified four point probe conductivity continue increasing, while the non-modified has suffered from a drastically decrease. Nonetheless, at 100 minutes, it is the SAM-modified sample which shows practically no conductivity. A possible explanation for these changes could be that a long exposure to iodine vapors can cause an overoxidation to the polymer, which can lead to the breakdown of the polymer backbone π-conjugation and thus, a loss of conductivity. Consequently, the exposure to iodine vapor has been established in 60 minutes as it seems time enough to perform the doping.

In general, the doping process has been a little bit misleading. There have appeared unexpected conductivity results as it has just been commented and some of them have varied despite of using the same experimental conditions. Plasma polymerization and exposure to iodine into the chamber influence clearly on final conductivity. Some alteration during these steps can result in an unpredicted state. Because of that, a possible improvement for the doping process that could be done in the future might be the *in-situ* monitoring of doping. It would be very adequate to control the change in conductivity by connecting somehow the four-point probe to the SourceMeter. Therefore, it would be possible to know at every moment the exact conductivity of the sample and therefore to achieve always the same level of doping to provide repeatable samples.

4.5 GAS MEASUREMENTS

Two different analytes, water vapor and carbon dioxide, were tested in order to study the operation and the viability of measuring vapors with the four-point probe. In order to perform the experiments a gas chamber has been designed. The most common way to express the results for a chemical sensor is using the sensitivity. The sensitivity is the ratio between the change in electrical resistance and initial resistance (Equation 10), which will be used to present the obtained results.

$$S = \frac{R_f - R_0}{R_0} \times 100 \tag{10}$$

where: R_f is the resistance in presence of the detected gas
R_0 is the resistance in pure air

4.5.1 GAS CHAMBER DESIGN

After testing different experimental conditions to find the most suitable, it was required the correct equipment to carry out the gas analysis. To measure conductivity changes due to the interaction of a vapor with the polymer, it was necessary to introduce the analyte in a controlled environment in which the amount of vapor flow can be monitored. Thus, a gas chamber has been designed to perform the conducting measurements of gases.

The gas chamber consists of a cylindrical vessel made of stainless steel, 16 cm length and 8.5 cm diameter. On the inside the walls are covered by TRIVOLTON®, a flexible multi-layer insulator produced as a three-layer combination: presspaper + polyester film + presspaper. The purpose is to isolate the electrical device and its stand from the metal chamber to avoid a circuit breaker. The cylinder is hermetically closed with a stainless steel top through a clamp. In the top, three male connectors (4 SS-6MO-1-2-W, Swagelok) were soldiered to be used as gas inlets and, moreover, a plug was placed to connect the stand, in which the electrode is located inside the gas chamber, with the Keithley 2611 System SourceMeter. Finally, at the back part of the gas chamber there is another male connector soldiered to be used as a gas outlet.

Figure 12. Image of the gas chamber (left) and the gas chamber connected to the Keithley 2611 System SourceMeter (right).

4.5.2 HUMIDITY

The first attempt in gas measurements was trying to investigate the conductivity change in PPy plasma polymerized films due to the introduction of water vapor inside the gas chamber. Humidity is a typical analyte due to the sensitivity of conducting polymers to it. [23-25] Moreover, because humidity can interfere with the measurement of other vapours by modifying the sensor sensitivity, it is important to study its effect since water molecules can compete with the odour molecules for the adsorption sites. The adsorption leads to the swelling of the polymer and then, to the corresponding drop in conductivity as it favours ionic conductivity.[26] Besides, depending on the amount of water adsorbed the conductivity can increase as a result of the proton exchange between PPy and adsorbed water molecules.[27] These changes can be due to small variations of the polymer backbone or environmental conditions.

Water vapor flows of 0.5 and 2 g/h were introduced into the gas chamber but none of them result in a conductivity change.

A possible explanation for this might be that the amount of water introduced was not enough to cause some effect in the polymer. According to Cruz[17] up to 70% of relative humidity there was no significant influence on conductivity on PPy plasma polymerized films. Another explanation could be that since plasma polymerization leads to highly cross-linked polymers, it makes the swelling process more difficult. As a consequence, if there is no swelling, there is no change in conductivity. Therefore, it means that water vapor does not affect the PPy electrical properties. What is more important, it means that the chemical sensor is stable under the atmospheric conditions tested and it is not affected by humidity.

4.5.3 CARBON DIOXIDE

Since CO_2 is involved in the most significant biological reactions, measuring carbon dioxide is important in monitoring indoor air quality and many industrial processes. Therefore, CO_2 was analyzed by using PPy plasma polymerized films as sensor.

¡Error! No se encuentra el origen de la referencia. displays the sensitivity response of two plasma polymerized films with different thickness. The idea is trying to find out whether the PPy films were sensitive to the analyte or not and if so, the differences between the two films.

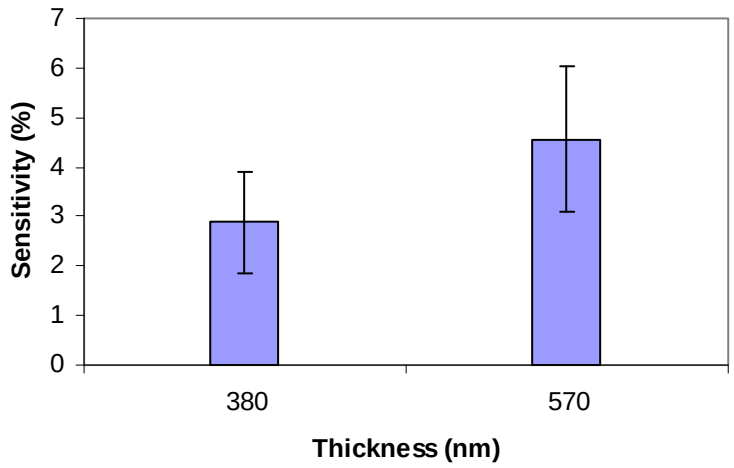

Figure 13. Sensitivity response of two PPy plasma polymerized films with a thickness of 380 and 570 nm to carbon dioxide.

It can be seen that exposure to CO_2 causes a variation of resistivity on the PPy plasma polymerized films, which means that this material offers chemical, physical and electrical properties that can be used for sensor applications. CO_2 in contact with the polymer has resulted in an increase in sensor resistance. The oxidized structure of PPy has two positive charges every four units of pyrrole. This bipolaron state is considered to be the charge carrier in the electronic transport mechanism. Besides, the dioxide carbon molecule has two lone pair of electrons for each C=O bond. The lone pair of electrons can interact with the positive charge on the PPy backbone forming reversible bonds and obtaining a reduce state of the polymer chain. Therefore, due to this interaction, it could be probable that polymer conductivity decreases.

Sensitivity values obtained are 2.9 and 4.6 for the 380 and 570 nm thick films. Besides, Waghuley *et al*[28] reported a maximum sensitivity value of 0.8 for chemically

synthesized conducting PPy films which were prepared by screen-printing technique to be used as a carbon dioxide gas sensor. Compared with the results found in our investigations, it seems that a higher sensitivity has been achieved, which encourage thinking that PPy plasma polymerized films can act as a gas sensor. Furthermore, a different sensitivity has been obtained depending on their thickness. Thicker films show a higher sensitivity which could stem from the fact that more CO_2 molecules can interact with the polymer and thus the resistance change is higher. This is very interesting as different responses are obtained with the same analyte. Studying the different responses of different sensors can lead to a characteristic pattern generation which will be used to create a database to identify and classify unknown analytes.

Finally, the reproducibility of the sensor has been tested by studying several adsorption-desorption cycles of CO_2 on a 570 nm thick PPy plasma polymerized film The result obtained can be observed in Figure 14.

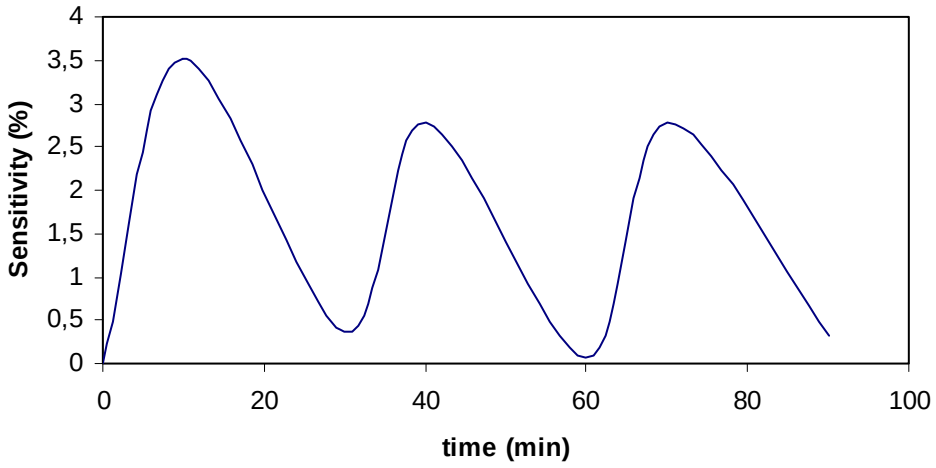

Figure 14. Resistivity response of the gas sensor based on a 570 nm thick PPy plasma polymerized film versus time.

Comparing the three cycles, the first one shows a slightly higher sensitivity in comparison with the other two, which show practically the same value. Moreover, the recovery process displays very similar values and it is quite close to the total recovery also. Even though CO_2 molecules have been bounded to the polymer, it seems that after a period of time they can be desorbed. Once the molecules have been displaced, the polymer can adopt again the bipolaron state and return to its initial electrical conductivity. Therefore, it can be assumed that the gas sensor presents a good reproducibility.

4.6 REFERENCES

1. Jonsson, S. K. M.; Birgerson, J.; Crispin, X.; Greczynski, G.; Osikowicz, W.; van der Gon, A. W. D.; Salaneck, W. R.; Fahlman, M. The effects of solvents on the morphology and sheet resistance in poly (3,4-ethylenedioxythiophene)-polystyrenesulfonic acid (PEDOT-PSS) films. *Synth. Met.* **2003,** *139* (1), 1-10.

2. Collier, J. H.; Camp, J. P.; Hudson, T. W.; Schmidt, C. E. Synthesis and characterization of polypyrrole-hyaluronic acid composite biomaterials for tissue engineering applications. *Journal of Biomedical Materials Research* **2000,** *50* (4), 574-584.

3. Norris, I. D.; Shaker, M. M.; Ko, F. K.; Macdiarmid, A. G. Electrostatic fabrication of ultrafine conducting fibers: polyaniline/polyethylene oxide blends. *Synth. Met.* **2000,** *114* (2), 109-114.

4. Armes, S. P.; Gottesfeld, S.; Beery, J. G.; Garzon, F.; Agnew, S. F. Conducting Polymer Colloidal Silica Composites. *Polymer* **1991,** *32* (13), 2325-2330.

5. Valdes, L. B. Resistivity Measurements on Germanium for Transistors. *Proceedings of the Institute of Radio Engineers* **1954,** *42* (2), 420-427.

6. Liau, Y. H.; Scherer, N. F.; Rhodes, K. Nanoscale electrical conductivity and surface spectroscopic studies of indium-tin oxide. *Journal of Physical Chemistry B* **2001,** *105* (16), 3282-3288.

7. Heim, T.; Deresmes, D.; Vuillaume, D. Conductivity of DNA probed by conducting-atomic force microscopy: Effects of contact electrode, DNA structure, and surface interactions. *J. Appl. Phys.* **2004,** *96* (5), 2927-2936.

8. Keller, S.; Mouaziz, S.; Boero, G.; Brugger, J. Microscopic four-point probe based on SU-8 cantilevers. *Rev. Sci. Instrum.* **2005,** *76* (12).

9. Ju, Y.; Ju, B. F.; Saka, M. Microscopic four-point atomic force microscope probe technique for local electrical conductivity measurement. *Rev. Sci. Instrum.* **2005,** *76* (8).

10. Petersen, C. L.; Hansen, T. M.; Boggild, P.; Boisen, A.; Hansen, O.; Hassenkam, T.; Grey, F. Scanning microscopic four-point conductivity probes. *Sensors and Actuators A-Physical* **2002,** *96* (1), II.

11. Huang, R. K.; Wang, C. A.; Harris, C. T.; Connors, M. K.; Shiau, D. A. Ohmic contacts to n-type GaSb and n-type GaInAsSb. *Journal of Electronic Materials* **2004,** 33 (11), 1406-1410.

12. Hirsch, J. Hopping Transport in Disordered Aromatic Solids - Reinterpretation of Mobility Measurements on Pkv and Tnf. *Journal of Physics C-Solid State Physics* **1979,** *12* (2), 321-335.

13. Wang, Z. H.; Scherr, E. M.; Macdiarmid, A. G.; Epstein, A. J. Transport and Epr Studies of Polyaniline - A Quasi-One-Dimensional Conductor with 3-Dimensional Metallic States. *Physical Review B* **1992,** *45* (8), 4190-4202.

14. Phillips, P.; Wu, H. L. Localization and Its Absence - A New Metallic State for Conducting Polymers. *Science* **1991,** *252* (5014), 1805-1812.

15. Zotti, G.; Zecchin, S.; Schiavon, G.; Berlin, A.; Pagani, G.; Canavesi, A. Conductivity in redox modified conducting polymers .2. Enhanced redox conductivity in ferrocene-substituted polypyrroles and polythiophenes. *Chem. Mater.* **1995,** *7* (12), 2309-2315.

16. Cassignol, C.; Olivier, P.; Ricard, A. Influence of the dopant on the polypyrrole moisture content: Effects on conductivity and thermal stability. *J. Appl. Polym. Sci.* **1998,** *70* (8), 1567-1577.

17. Cruz, G. J.; Morales, J.; Olayo, R. Films obtained by plasma polymerization of pyrrole. *Thin Solid Films* **1999,** *342* (1-2), 119-126.

18. Wang, W.; Lee, T.; Reed, M. A. Elastic and Inelastic Electron Tunneling in Alkane Self-Assembled Monolayers. *The Journal of Physical Chemistry B* **2004,** *108* (48), 18398-18407.

19. Wang, W. Y.; Lee, T.; Reed, M. A. Electron tunnelling in self-assembled monolayers. *Reports on Progress in Physics* **2005,** *68* (3), 523-544.

20. Boulas, C.; Davidovits, J. V.; Rondelez, F.; Vuillaume, D. Suppression of charge carrier tunneling through organic self-assembled monolayers. *Phys. Rev. Lett.* **1996,** *76* (25), 4797-4800.

21. Wuelfing, W. P.; Murray, R. W. Electron Hopping through Films of Arenethiolate Monolayer-Protected Gold Clusters. *The Journal of Physical Chemistry B* **2002,** *106* (12), 3139-3145.

22. Zamborini, F. P.; Leopold, M. C.; Hicks, J. F.; Kulesza, P. J.; Malik, M. A.; Murray, R. W. Electron Hopping Conductivity and Vapor Sensing Properties of Flexible Network Polymer Films of Metal Nanoparticles. *J. Am. Chem. Soc.* **2002,** *124* (30), 8958-8964.

23. Suri, K.; Annapoorni, S.; Sarkar, A. K.; Tandon, R. P. Gas and humidity sensors based on iron oxide-polypyrrole nanocomposites. *Sensors and Actuators B-Chemical* **2002,** *81* (2-3), 277-282.

24. Chakraborty, M.; Mukherjee, D. C.; Mandal, B. M. Interpenetrating polymer network composites of polypyrrole and poly(vinyl acetate). *Synth. Met.* **1999,** *98* (3), 193-200.

25. Collins, G. E.; Buckley, L. J. Conductive polymer-coated fabrics for chemical sensing. *Synth. Met.* **1996,** *78* (2), 93-101.

26. Cho, J. H.; Yu, J. B.; Kim, J. S.; Sohn, S. O.; Lee, D. D.; Huh, J. S. Sensing behaviors of polypyrrole sensor under humidity condition. *Sensors and Actuators B-Chemical* **2005,** *108* (1-2), 389-392.

27. Geng, W.; Li, N.; Li, X.; Wang, R.; Tu, J.; Zhang, T. Effect of polymerization time on the humidity sensing properties of polypyrrole. *Sensors and Actuators B: Chemical* **2007,** *125* (1), 114-119.

28. Waghuley, S. A.; Yenorkar, S. M.; Yawale, S. S.; Yawale, S. P. Application of chemically synthesized conducting polymer-polypyrrol as a carbon dioxide gas sensor. *Sensors and Actuators B: Chemical* **2008,** *128* (2), 366-373.

CHAPTER 5

CONCLUSIONS

5. CONCLUSIONS

The present thesis has been focused on surface modification to deposit conducting polymers by plasma chemical vapor deposition. According to the thesis's objectives the next conclusions have been reached.

1. Different series of organic compounds with a pyrrole terminated group to form self-assembled monolayers on gold, copper and silicon surfaces have been synthesized. The monolayer quality has been deeply studied by surface characterization techniques and electrochemical methods. The monolayers formed have shown to be well-structured, densely packed and have shown their protective efficiency against corrosion. Moreover, monolayers with the longest alkyl chain have provided the best results since they present a higher structural order due to methylenes' Van der Waals interactions among chains.

2. The pyrrole-terminated group in the monolayer acts as a nucleation promoter in plasma chemical vapor deposition of polypyrrole. Atomic Force Microscopy has revealed that the pyrrole-terminated group enhances the nucleation-growth mechanism in plasma polymerization. Polypyrrole nuclei were deposited more preferably on SAM-modified surfaces and the growth of these nuclei has resulted in more homogeneous films.

3. Plasma polymerized polypyrrole films have been synthesized using different duty cycles. The deposition rate has ranged from 9 to 19 nm/min. Studying the presence of the aromatic amine into the polymer structure has revealed a high retention of functionality in all the films, although plasma conditions. Furthermore, XPS and FT-IR analysis have demonstrated the incorporation of iodide into the polymer backbone by exposing the films to iodine vapor.

4. Monolayers have shown a major influence on polymer deposition when studying the nucleation-growth mechanism than on thicker polypyrrole films formation. Nevertheless, polypyrrole plasma polymerized films have presented better adhesion properties on previously SAM-modified substrates.

5. A novel four-point probe configuration has been designed and integrated into a printed circuit board to measure conductivities on thin films. Different electrode configurations with different area and shape were tested in order to optimize the measurement, resulting in an easy and cheap way to study the electrical properties of materials.

6. The conductive form of polypyrrole has been obtained by polymer oxidation through iodine vapor exposure. The experimental conditions for the doping process and for the electrical measurement were investigated obtaining polypyrrole films with a conductivity of 40 S/cm. Moreover, the electrical properties have remained steady for a period of time longer than 20 days.

7. Gas analysis of humidity and carbon dioxide have been carried out using polypyrrole plasma thin films deposited on the four-point probe in a gas chamber built for this particular purpose. In the experimental conditions tested, the polypyrrole films have presented a stable behaviour under humidity. Furthermore, the chemical sensor has exhibited high sensitivity to carbon dioxide exposure. It has shown sensitivity values of 2.9 and 4.6 depending on the film thickness. Thus, polypyrrole plasma polymerized films have significantly demonstrated their utility as a chemical sensor for carbon dioxide measurements.

5. CONCLUSIONES

La presente tesis se ha centrado en la modificación de superficies para depositar un polímero conductor mediante deposición química en fase vapor por plasma. De acuerdo a los objetivos planteados en la tesis, se ha llegado a las siguientes conclusiones:

1. Se ha sintetizado una serie de compuestos orgánicos con un grupo pirrol terminal para formar monocapas auto-ensambladas sobre superficies de oro, cobre y silicio. La calidad de las monocapas ha sido estudiada por diversas técnicas de caracterización de superficies y métodos electroquímicos. Las monocapas formadas han mostrado estar bien estructuradas, altamente compactas y tener una alta eficiencia contra la corrosión. Además las monocapas con la cadena alquílica más larga presentan una mayor calidad debido a un mayor orden estructural como consecuencia de las interacciones de Van der Waals entre los metilenos de las cadenas.

2. El grupo terminal pirrol de la monocapa actúa como promotor de la nucleación en la deposición de polipirrol por deposición química en fase vapor por plasma. La Microscopía de Fuerza Atómicas ha revelado que este grupo pirrol mejora el mecanismo de nucleación-crecimiento en la polimerización por plasma. Los núcleos de polipirrol han sido depositados preferentemente en las superficies modificadas con monocapas y el crecimiento de estos núcleos da lugar a películas más homogéneas.

3. Las películas de polipirrol polimerizadas por plasma han sido sintetizadas usando diferentes ciclos de trabajo. La velocidad de deposición ha variado entre 9 y 19 nm/min. Mediante el estudio de la amina aromática de la estructura del polímero se ha demostrado una alta retención de la funcionalidad del polipirrol en todas las películas a pesar de las condiciones de plasma. Además, los análisis de XPS y FT-IR han demostrado la incorporación de ioduro dentro de la estructura del polímero mediante la exposición de las películas a vapores de yodo.

4. Las monocapas han causado una mayor influencia en la deposición del polímero cuando se ha estudiado el mecanismo de nucleación-crecimiento, en comparación con la formación de películas de polipirrol más gruesas. De todas formas, las películas de polipirrol sintetizadas por plasma han demostrado tener mejores propiedades de adhesión en aquellos sustratos que habían sido previamente modificados con una monocapa.

5. Se ha diseñado una nueva configuración para la sonda de cuatro puntas y se ha incorporado como parte de un circuito impreso para la medida de conductividad en películas delgadas. Se han examinado distintas configuraciones y electrodos con diferentes áreas y formas para optimizar las medidas, obteniendo un método fácil y barato para estudiar las propiedades eléctricas de los materiales.

6. Se ha obtenido la forma conductora del polipirrol a través de la oxidación del polímero mediante la exposición a vapores de yodo. Se han investigado las condiciones experimentales para el proceso de dopaje y para las medidas eléctricas obteniéndose películas de polipirrol con una conductividad de 40 S/cm. Asimismo, las propiedades eléctricas se han mantenido estables por un periodo de tiempo superior a los 20 días.

7. Se ha llevado a cabo análisis de humedad y de dióxido de carbono usando películas delgadas de polipirrol depositadas sobre la sonda de cuatro puntas en una cámara de gases diseñada especialmente para dicho propósito. En las condiciones en las cuales se han realizado los experimentos, las películas de polipirrol presentan un comportamiento estable frente a la humedad. Además, el sensor químico ha mostrado una alta sensibilidad a la exposición de dióxido de carbono y se ha obtenido unos valores de sensibilidad de 2.9 y 4.6 en función del grosor de la película. Por consiguiente, se ha demostrado la capacidad de las películas de polipirrol sintetizadas por plasma para ser utilizadas como sensor químico para la determinación de dióxido de carbono.

5. CONCLUSIONS

La present tesis s'ha centrat en la modificació de superfícies per dipositar un polímer conductor mitjançant deposició química en fase vapor per plasma. D'acord amb els objectius plantejats a la tesi, s'han assolit les següents conclusions:

1. S'ha sintetitzat una sèrie de compostos orgànics amb un grup pirrol terminal per formar monocapes auto-assemblades sobre superfícies d'or, coure i silici. La qualitat de les monocapes ha estat estudiada per diverses tècniques de caracterització de superfícies i mètodes electroquímics. Les monocapes formades han mostrat estar ben estructurades, ser altament compactes i tenir una bona eficiència contra la corrosió. A més, les monocapes amb la cadena alquílica més llarga presenten millors resultats degut a un major ordre estructural com a conseqüència de les interaccions de Van der Waals entre els metilens de les cadenes.

2. El grup terminal pirrol de la monocapa actua com a promotor de la nucleació a la deposició de polipirrol per deposició química en fase vapor per plasma. La Microscopia de Forces Atòmiques ha revelat que aquest grup pirrola millora el mecanisme de nucleació-creixement en la polimerització per plasma. Els nuclis de polipirrol es dipositen preferentment sobre les superfícies modificades amb monocapes i el creixement d'aquests nuclis dona lloc a pel·lícules més homogènies.

3. Les pel·lícules de polipirrol polimeritzades per plasma han estat sintetitzades fent servir diferents cicles de treball. La velocitat de deposició ha variat entre 9 i 19 nm/min. Mitjançant l'estudi de l'amina aromàtica de l'estructura del polímer s'ha demostrat una alta retenció de la funcionalitat del polipirrol a totes les pel·lícules malgrat les condicions de plasma. A més, les anàlisis de XPS o FT-IR han demostrat la introducció de iodur dins de l'estructura del polímer mitjançant l'exposició de les pel·lícules a vapors de iode.

4. Les monocapes han causat una major influència en la deposició del polímer quan s'ha estudiat el mecanisme de nucleació-creixement, en comparació amb la formació de pel·lícules de polipirrol més gruixudes. De totes maneres, les pel·lícules de polipirrol sintetitzades per plasma han demostrat tenir millors propietats adhesives sobre aquells substrats que prèviament havien estat modificades amb una monocapa.

5. S'ha dissenyat una nova configuració per la sonda de quatre puntes i s'ha incorporat com un element més a un circuit imprès per a la mesura de conductivitat en pel·lícules primes. S'han examinat diverses configuracions i elèctrodes amb diferents àrees i formes per optimitzar el sistema de mesura, obtenint un mètode fàcil i barat per estudiar les propietats elèctriques dels materials.

6. S'ha obtingut la forma conductora del polipirrol a través de l'oxidació del polímer mitjançant l'exposició a vapors de iode. S'ha investigat les condicions experimentals per al procés de dopatge i per a les mesures elèctriques obtenint pel·lícules de polipirrol amb una conductivitat de 40 S/cm. Així mateix, les propietat elèctriques s'han mantingut estables durant un període de temps superior a vint dies.

7. S'ha dut a terme anàlisis d'humitat i de diòxid de carboni fent servir pel·lícules primes de polipirrol dipositades sobre la sonda de quatre puntes en una cambra de gasos dissenyada especialment per a l'esmentat propòsit. En les condicions en les quals s'han realitzat els experiments, les pel·lícules de polipirrol presenten un comportament estable davant la humitat. A més el sensor químic ha mostrat una alta sensibilitat a l'exposició de diòxid de carboni i s'ha obtingut uns valors de sensibilitat de 2.9 i 4.6 en funció del gruix de la pel·lícula. Per tant, s'ha demostrat la capacitat de les pel·lícules de polipirrol sintetitzades per plasma per ser utilitzades com a sensor químic per a la determinació de diòxid de carboni.

CHAPTER 6

ANNEXES

6. ANNEXES

In this chapter, the results omitted, basically due to repetition, have been included. The ^{1}H-MNR and FT-IR spectra of the target molecules are shown. Additionally, FT-IR and XPS spectra of PPy plasma polymerized thin films can be observed.

6.1 PROTON NUCLEAR MAGNETIC RESONANCE

- **N-(6-Bromo)hexylpyrrole**

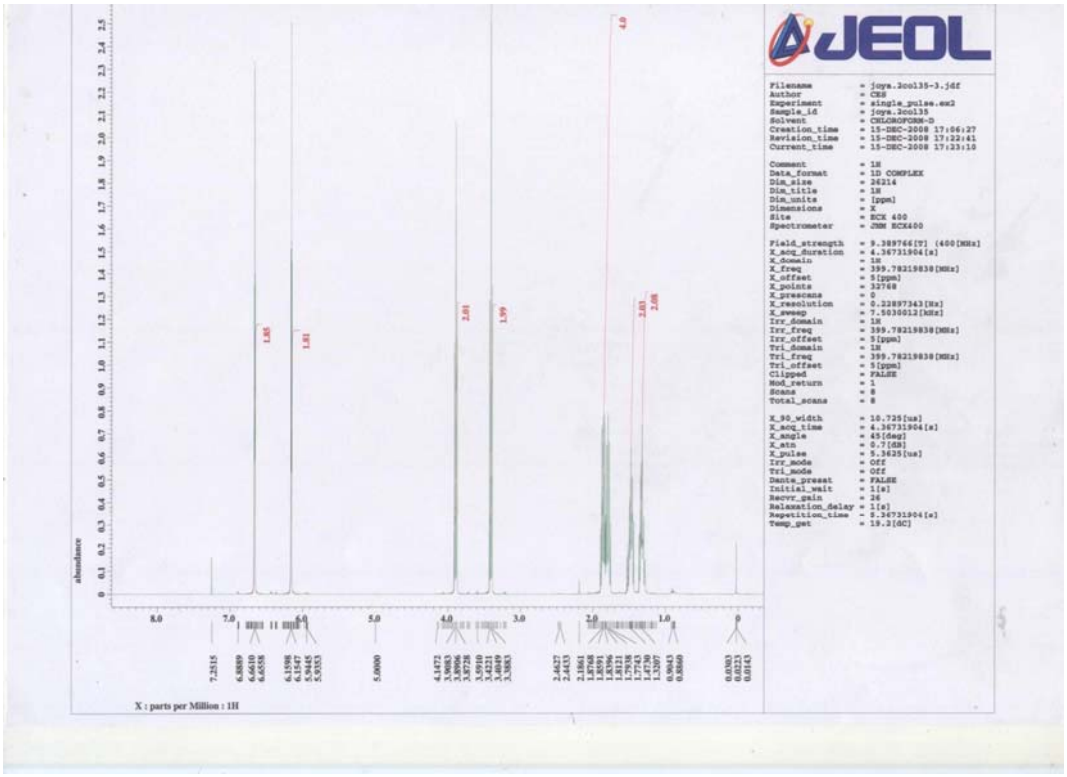

Figure 1. ^{1}H-NMR of N-(6-Bromo)hexylpyrrole.

- **N-(12-Bromo)dodecylpyrrole**

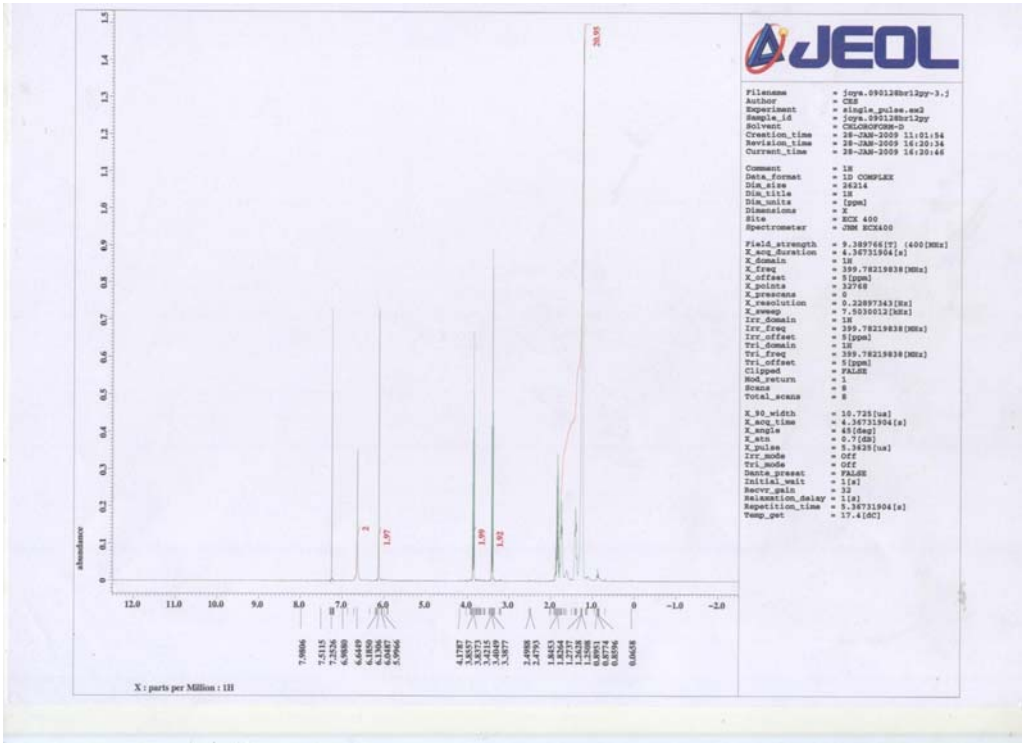

Figure 2. ^{1}H-NMR of N-(12-Bromo)dodecylpyrrole.

- **6-(N-pyrrolyl)hexanethiol**

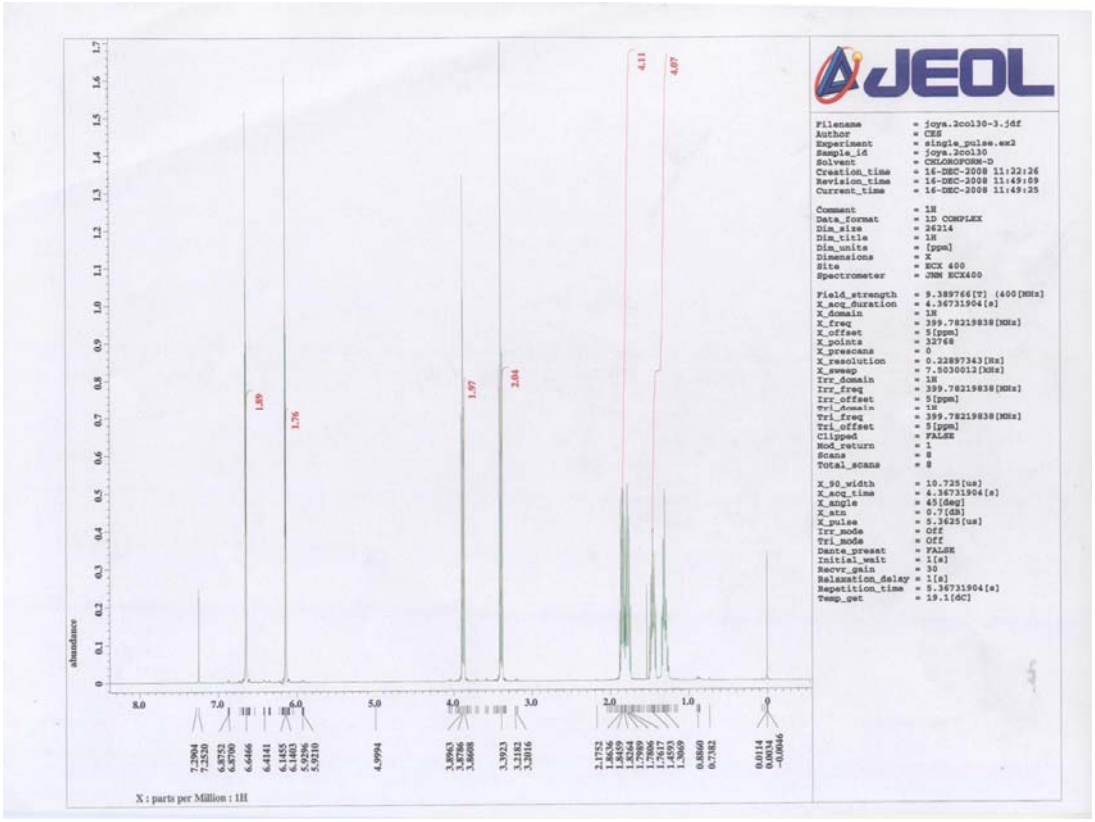

Figure 3. ^{1}H-NMR of 6-(N-pyrrolyl)hexanethiol.

- **12-(N-pyrrolyl)dodecanethiol**

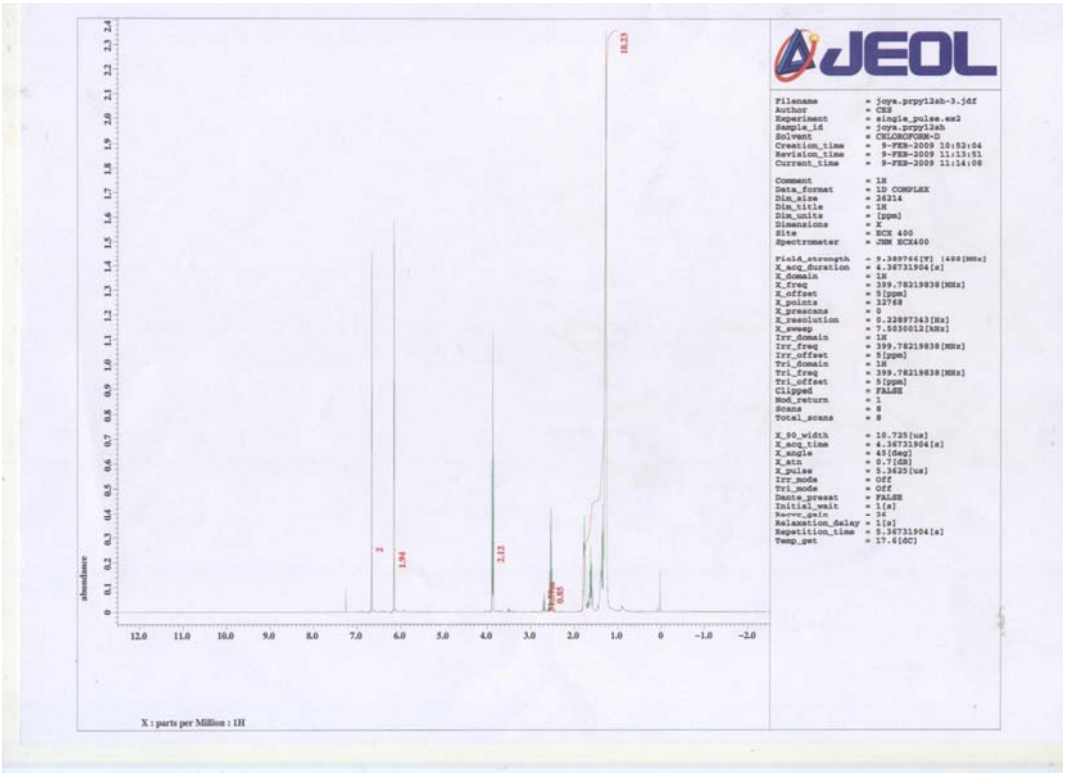

Figure 4. ^{1}H-NMR of 12-(N-pyrrolyl)dodecanethiol.

- **6-(N-pyrrolyl)hexaneselenol**

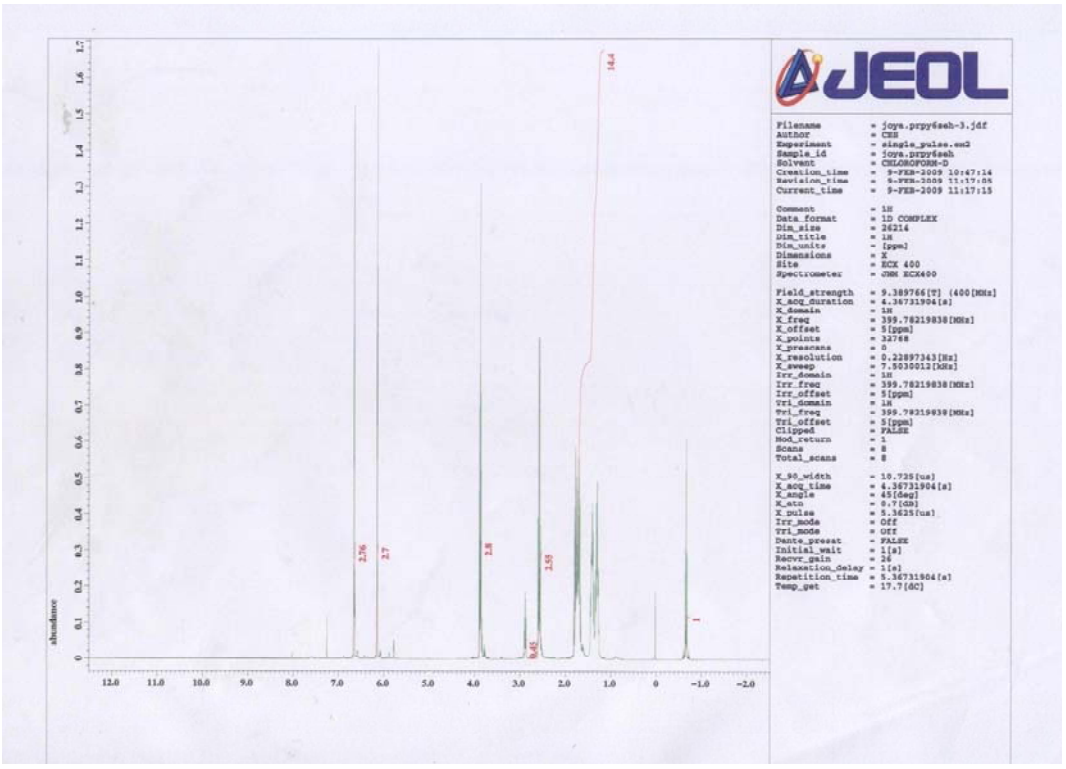

Figure 5. ^{1}H-NMR of 6-(N-pyrrolyl)hexaneselenol.

- **12-(N-pyrrolyl)dodecaneselenol**

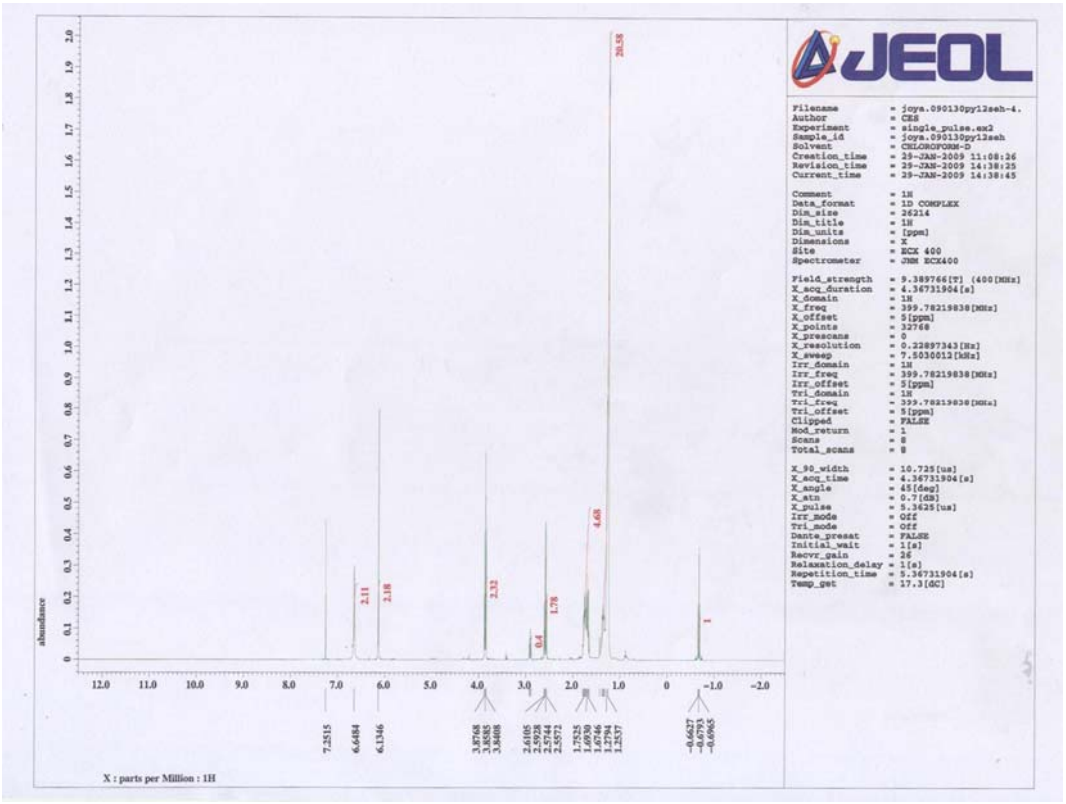

Figure 6. ^{1}H-NMR of 12-(N-pyrrolyl)dodecaneselenol.

- **11-(pyrrol-1-yl-undecyl)dimethylchlorosilane**

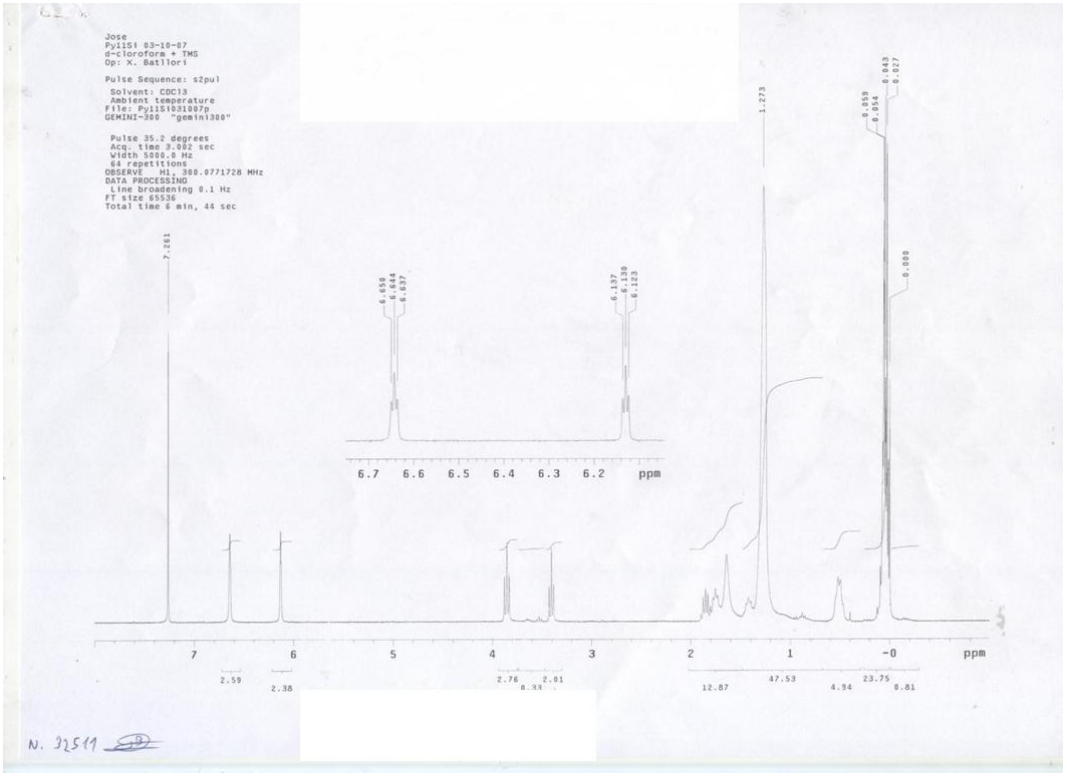

Figure 7. 1H-NMR of 11-(pyrrol-1-yl-undecyl)dimethylchlorosilane.

6.2 FOURIER TRANSFORM INFRARED

- **6-(N-pyrrolyl)hexanethiol**

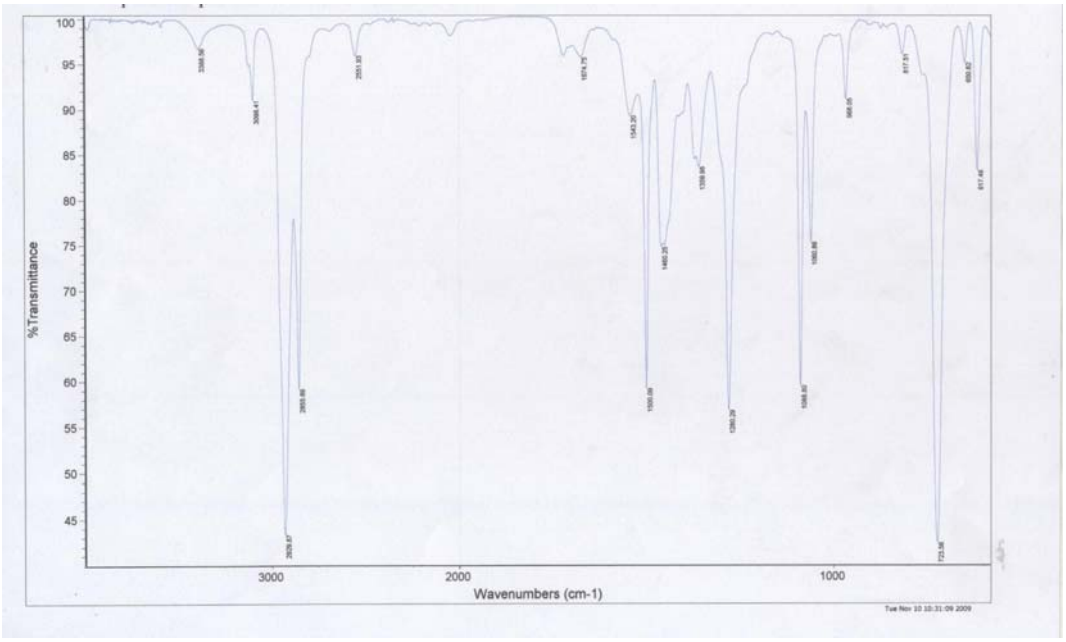

Figure 8. FT-IR of 6-(N-pyrrolyl)hexanethiol.

- **12-(N-pyrrolyl)dodecanethiol**

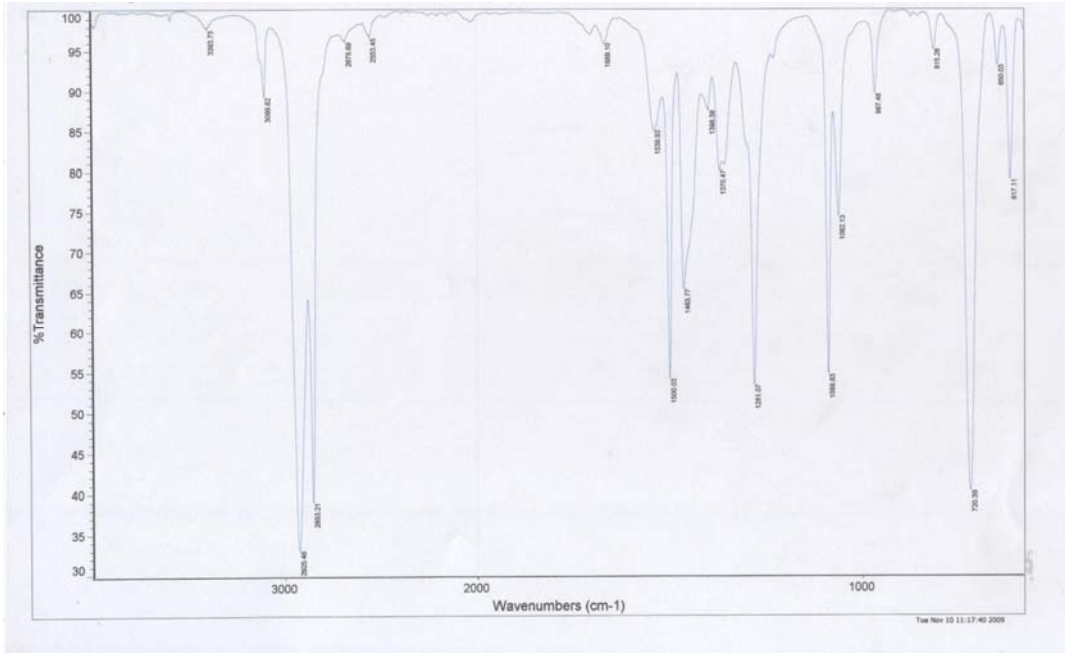

Figure 9. FT-IR of 12-(N-pyrrolyl)dodecanethiol.

- **6-(N-pyrrolyl)hexaneselenol**

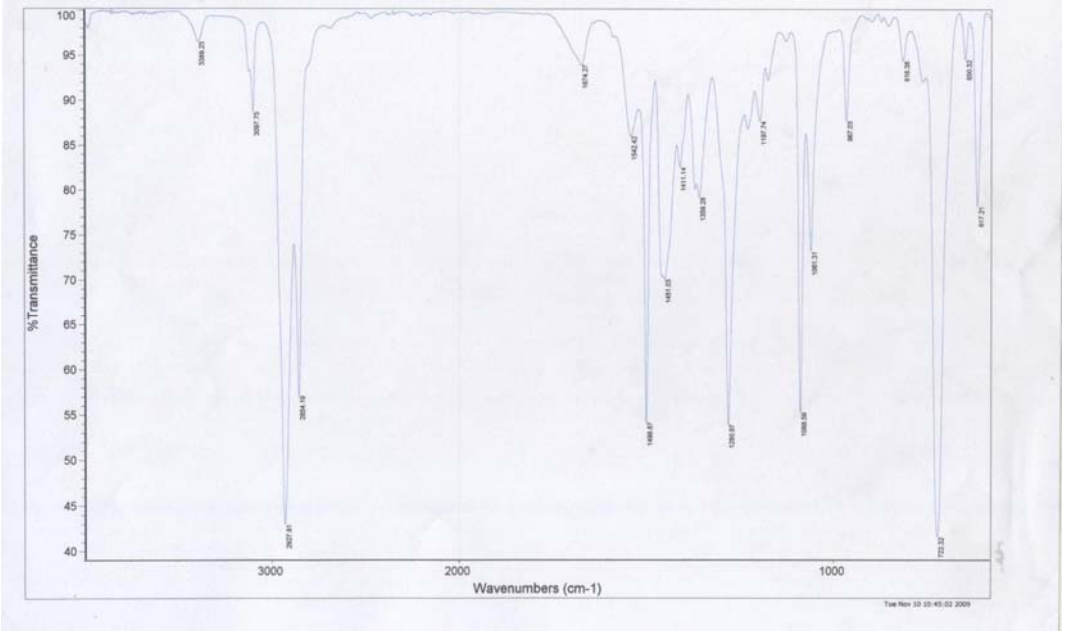

Figure 10. FT-IR of 6-(N-pyrrolyl)hexaneselenol.

- **12-(N-pyrrolyl)dodecaneselenol**

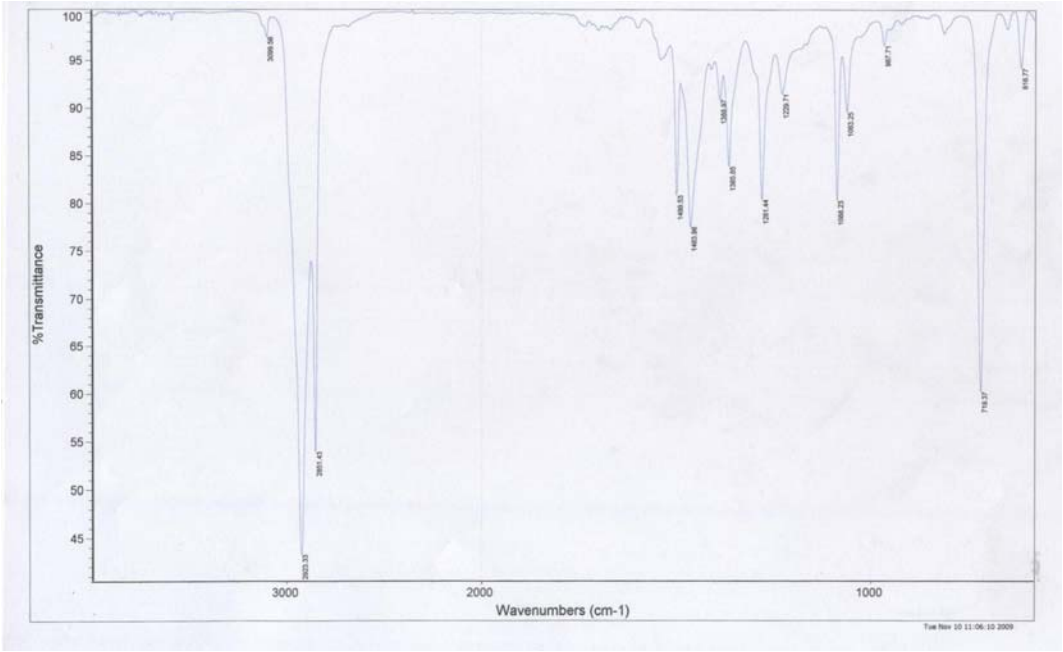

Figure 11. FT-IR of 12-(N-pyrrolyl)dodecanethiol.

- **11-(N-pyrrolyl)undecene**

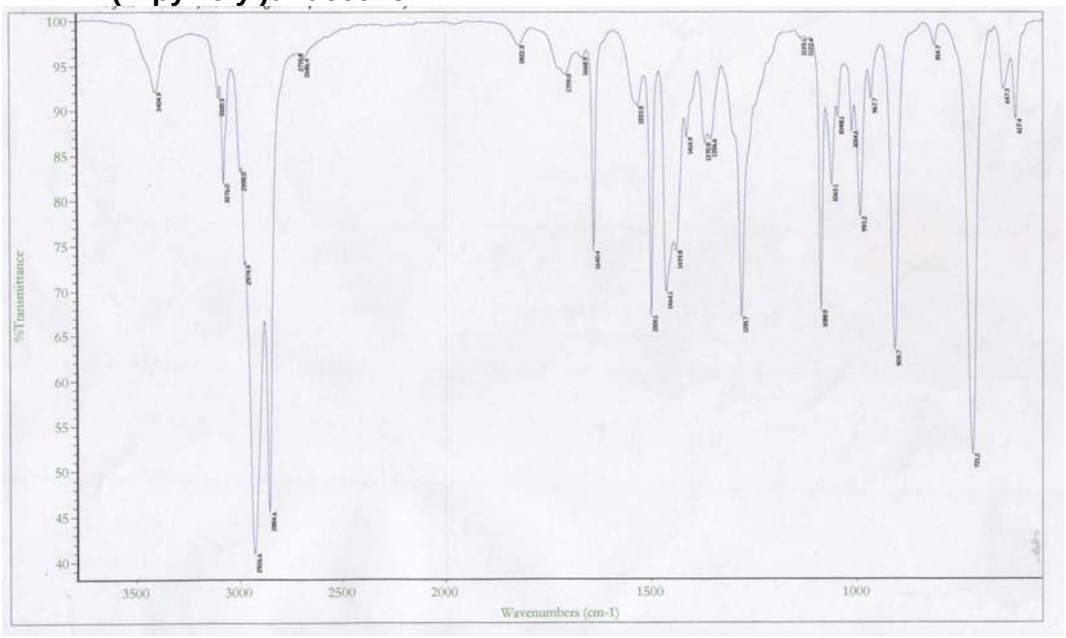

Figure 12. FT-IR of 11-(N-pyrrolyl)undecene.

- **11-(pyrrol-1-yl-undecyl)dimethylchlorosilane**

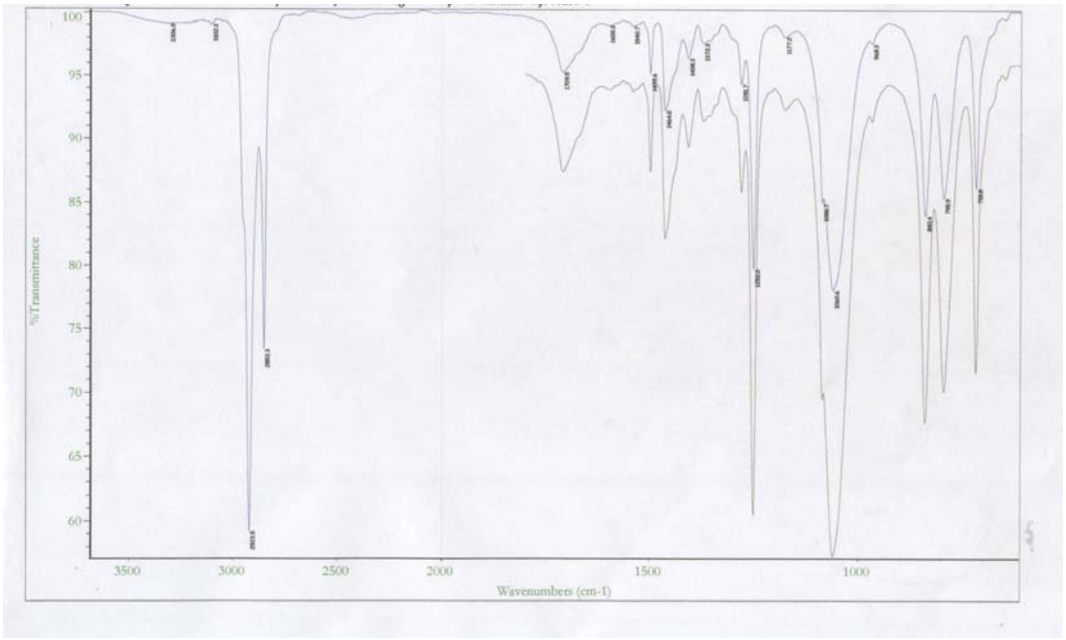

Figure 13. FT-IR of 11-(pyrrol-1-yl-undecyl)dimethylchlorosilane.

- **Plasma polymerized films for 5 min at different duty cycles**

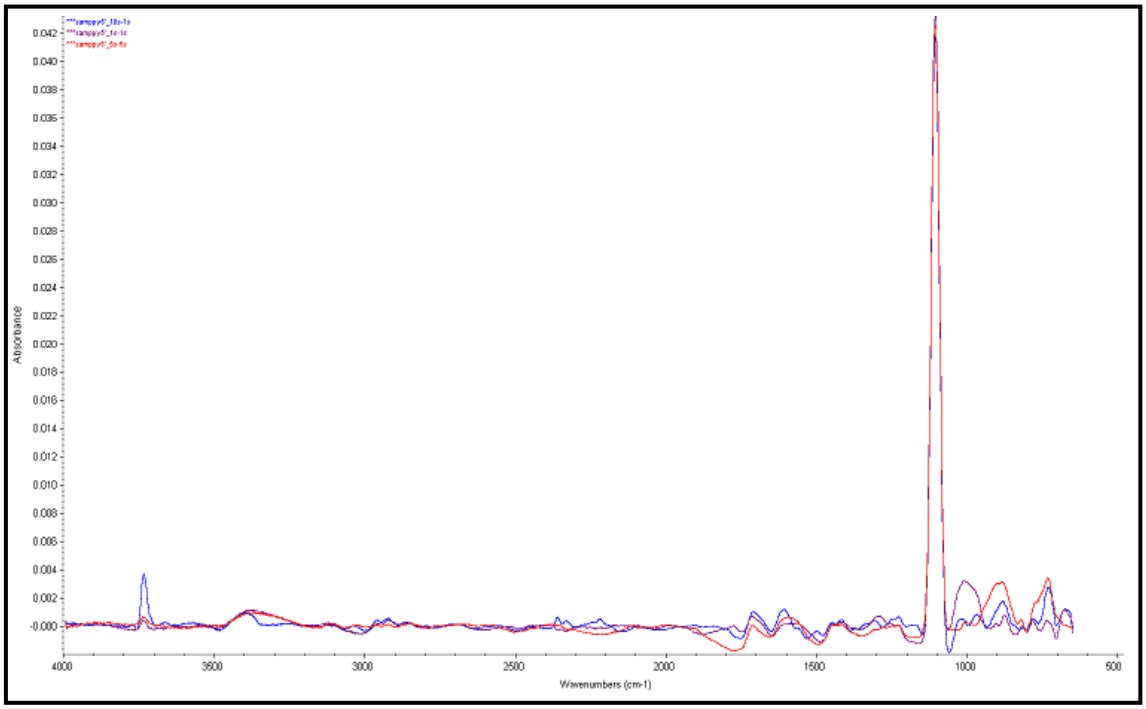

Figure 14. FT-IR spectra of plasma polymerized films on SAM-modified silicon surfaces deposited after 5 min with different duty cycles: 90% (10s ON / 1s OFF) blue line, 50% (5s ON / 5s OFF) red line and 50% (1s ON / 1s OFF) violet line.

- **Plasma polymerized films at duty cycle of 50%at different times**

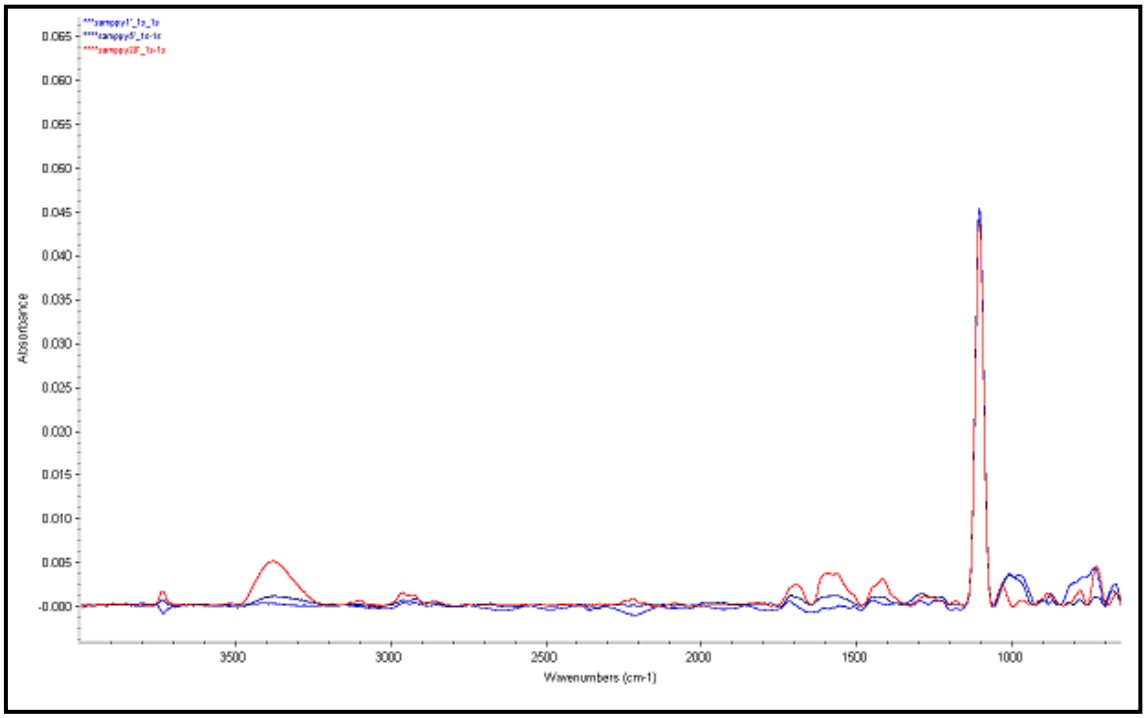

Figure 15. FT-IR spectra of plasma polymerized films with a 50% (1s ON / 1s OFF) duty cycle polymerized at different times: 1 min (blue line), 5 min (violet line) and 20 min (red line).

6.3 X-ray photoelectron spectroscopy

- **Py6SH SAM-modified copper polymerized for 1 min.**

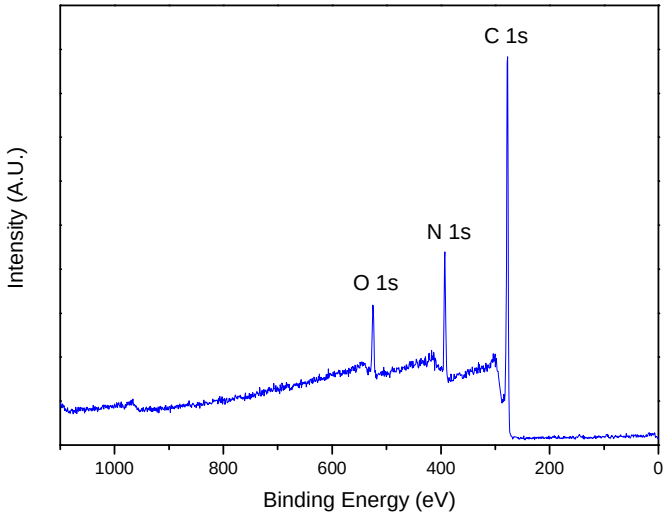

Figure 16. XPS spectrum of Py6SH SAM-modified copper polymerized for 1 min.

- **Py6SeH SAM-modified copper polymerized for 1 min.**

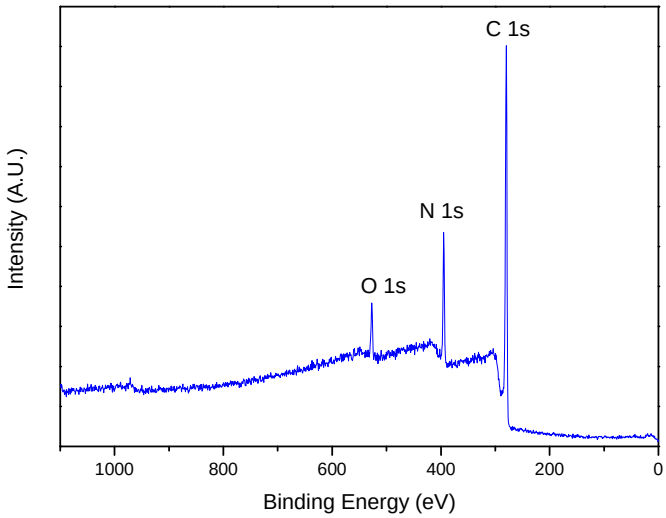

Figure 17. XPS spectrum of Py6SeH SAM-modified copper polymerized for 1 min.

- **Py12SeH SAM-modified copper polymerized for 1 min.**

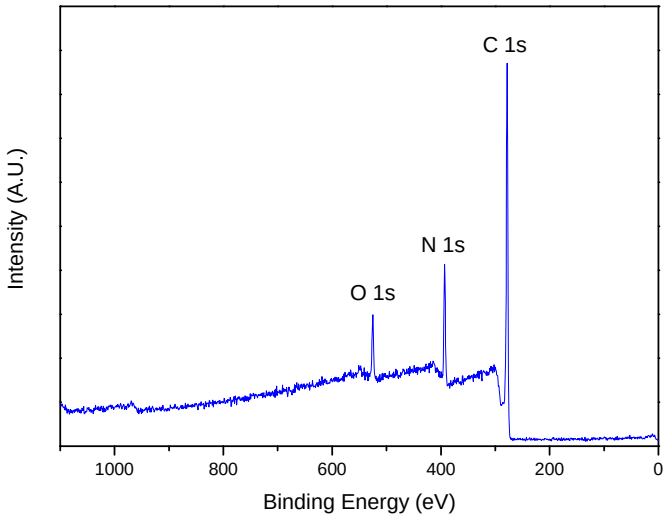

Figure 18. XPS spectrum of Py12SeH SAM-modified copper polymerized for 1 min.

Deconvolution analysis

- **Deconvolution of N 1s spectra of Py6SH SAM polymerized for 1min**

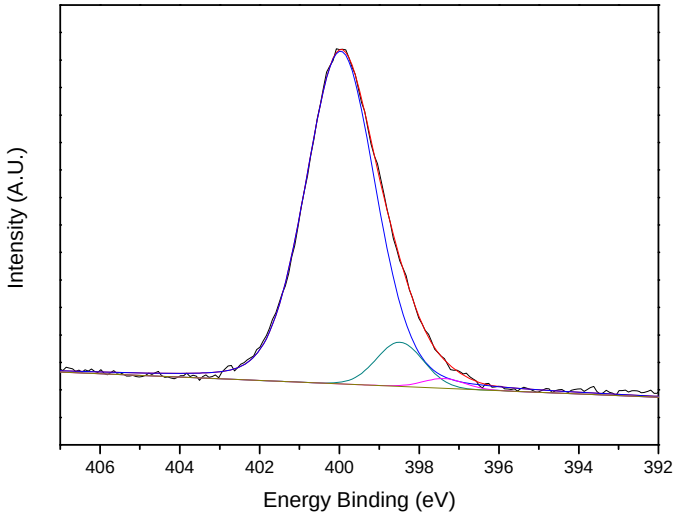

Figure 19. N 1s high resolution XPS spectrum of Py6SH SAM polymerized for 1 min.

- **Deconvolution of N 1s spectra of Py6SeH SAM polymerized for 1min**

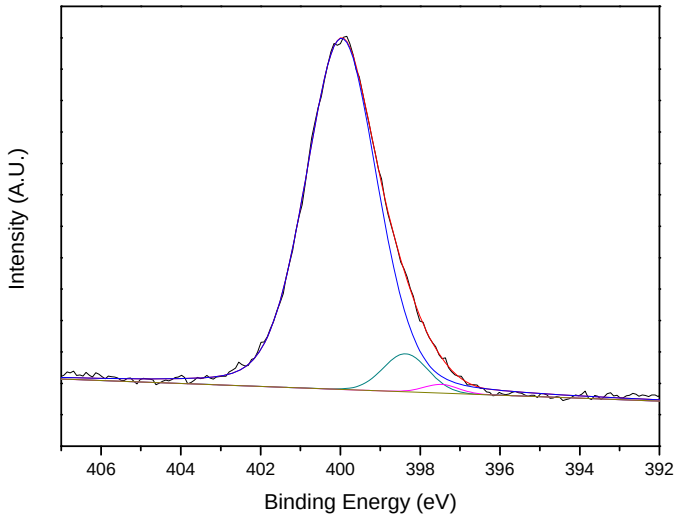

Figure 20. N 1s high resolution XPS spectrum of Py6SeH SAM polymerized for 1 min.

- **Deconvolution of N 1s spectra of Py12SeH SAM polymerized for 1min**

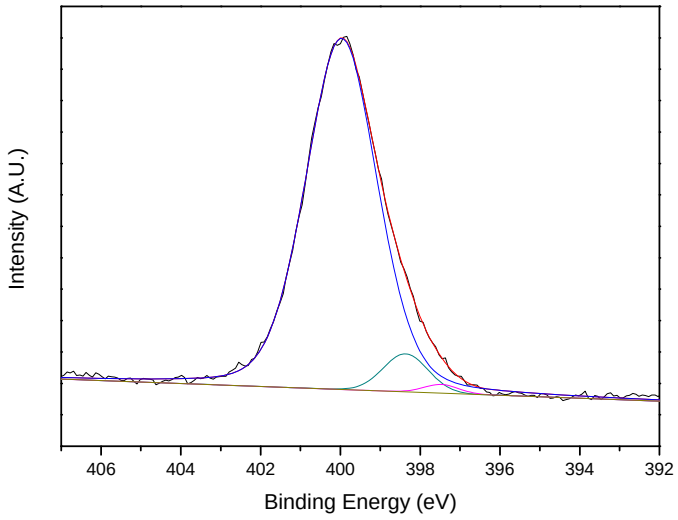

Figure 21 N 1s high resolution XPS spectrum of Py12SeH SAM polymerized for 1 min.

- **Deconvolution of C 1s spectra of Py6SH SAM polymerized for 1min**

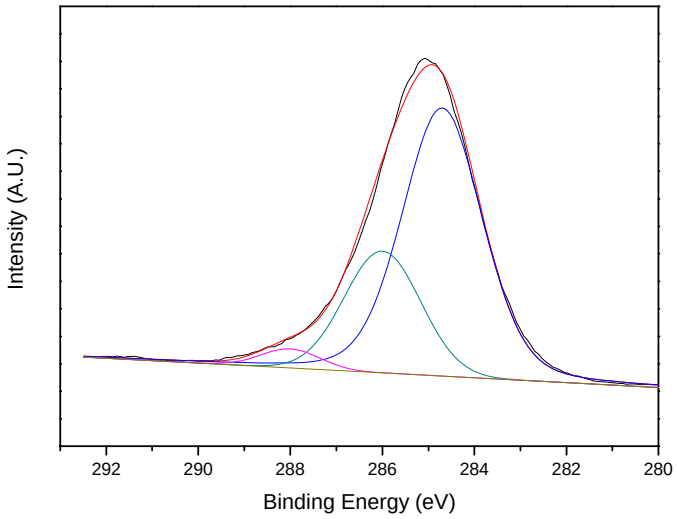

Figure 22. C 1s high resolution XPS spectrum of Py6SH SAM polymerized for 1 min.

- **Deconvolution of C 1s spectra of Py6SeH SAM polymerized for 1min**

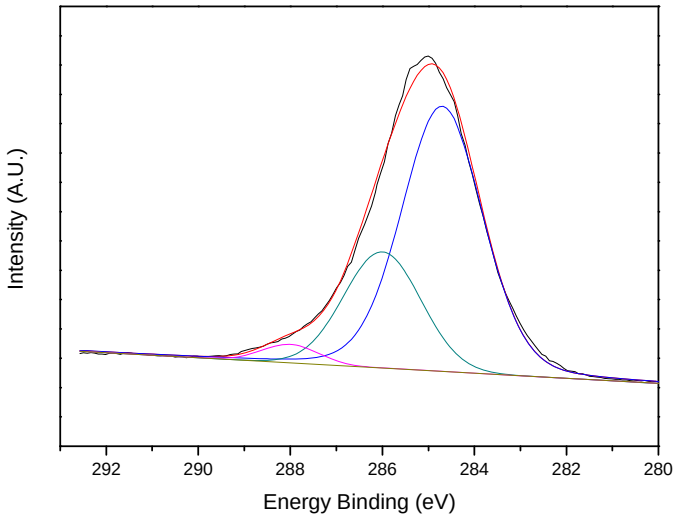

Figure 23. C 1s high resolution XPS spectrum of Py6SeH SAM polymerized for 1 min.

- **Deconvolution of C 1s spectra of Py12SeH SAM polymerized for 1min**

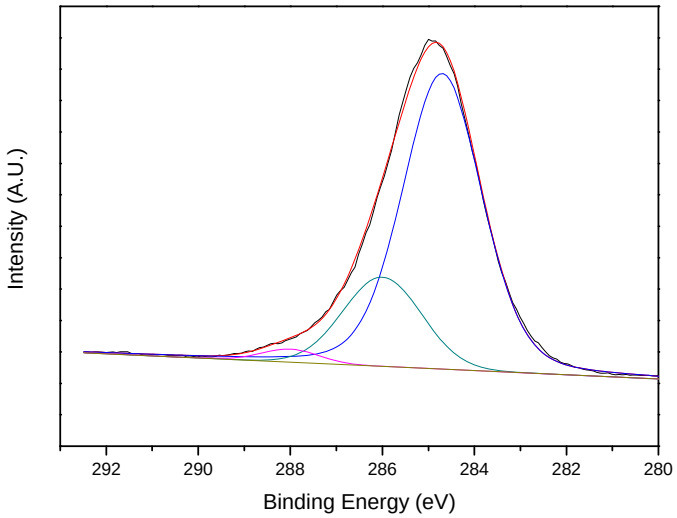

Figure 24. C 1s high resolution XPS spectrum of Py12SeH SAM polymerized for 1 min.

BIBLIOGRAPHY

PUBLISHED PAPERS

- *Plasma polymerization of polypyrrole-like films on nanostructured surfaces*
  J. L. Yagüe, N. Agullo, S. Borros
  Plasma Processes and Polymers, **2008**, Volume 5 Issue 5, Pages 433-443.

- *Growth of Polypyrrole-like Films on Self-Assembly Nanostructured Silicon Surfaces by PECVD*
  J. L. Yagüe, N. Agullo, S. Borros
  Chemical Vapor Deposition, **2009**, Volume 15, Issue 4-6, Pages 128-132.

- *Thiol vs selenol SAMs as nucleation enhancers and adhesion promoters for plasma polymerized pyrrole on copper substrates*
  J. L. Yagüe, N. Agullo, G. Fonder, J. Delhalle, Z. Mekhalif, S. Borros
  Plasma Processes and Polymers, Published online **Mar 31 2010** DOI: 10.1002/ppap.200900178.

- *A new four-point probe design to measure conductivity in polymeric thin films*
  J.L. Yagüe, A. Guimerà, R. Villa, N. Agulló, S. Borrós
  Plasma processes and Polymers, **2010**, submitted.

PAPERS IN PREPARATION

- *Doping of plasma polymerized polypyrrole films: study of the incorporation of iodine into the polymer's backbone*

ORAL COMMUNICATIONS

- *Nanostructured surfaces by organic conducting thin films for sensor applications*
  J. L. Yagüe, S. Borrós
  E-MRS 2006 Spring Meeting. Nice, France. June 2006

- *Polypyrrole synthesis through plasma assisted polymerization on nanostructured surfaces*
  J. L. Yagüe, S. Borrós
  IX National Meeting of Materials. Vigo, Spain. June 2006

- *A novel method to obtain polypyrrole-like thin films by plasma-enhanced chemical vapor deposition*
  J. L. Yagüe, S.Borrós
  10th European High Temerature Plasma Processes Conference. Patras, Greece. July 2008

- *Nanostructuration of PPy thin films deposited by PECVD for development of a gas sensor*
  J. L. Yagüe, S. Borrós
  VI Trobada de Joves Investigadors del Països Catalans. Valencia, Spain. 01-02 February 2010

POSTER PRESENTATIONS

- *Developing of conducting polymers thin films by plasma assisted polymerization on nanostructured surfaces*
  J. L. Yagüe, N. Agulló, S. Borrós
  Nanofabrication Conferences. Barcelona, Spain. November 2006

- *Development of nanostructured conducting polymer thin film by plasma enhanced CVD*
  J. L. Yagüe, N. Agulló, S. Borrós
  EuroCVD-16, The Hague, Netherlands, Setember 2007

- *Development of a novel probe design for the four-point probe method to study conducting polymers thin films synthesized by PECVD*
  J. L. Yagüe, N. Agulló, S. Borrós
  Third International School of Advanced Plasma Technology. Varenna, Italy.July 2008

- *Surface nanostructuration to increase polypyrrole adhesion deposited by PECVD*
  J. L. Yagüe, N.Agulló, Z. Mekhalif, S. Borrós
  TNT 2009, Trends in NanoTechnology. Barcelona, Spain. September 2009